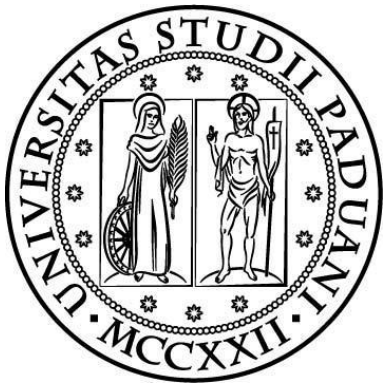

UNIVERSITÀ DEGLI STUDI DI PADOVA
DIPARTIMENTO DI INGEGNERIA INDUSTRIALE
CORSO DI LAUREA IN INGEGNERIA DEI MATERIALI

Post-processing treatments for improving the wear resistance of FSPed Al-matrix composite

Promoter: Prof. IRENE CALLIARI
Co - Promoter: Dr. (Research Associate) ANNE MERTENS
Prof. JACQUELINE LECOMTE-BECKERS

Marco Storti
Master Thesis

Academic Year 2015/2016

Abstract

This work investigates the wear properties of an aluminum metal matrix composite made of a 6005A matrix with short carbon fibers used as reinforcement, in particular the effect of thermal treatments and of the reinforcement. The material was produced by friction stir processing a sandwich made of two aluminum plates with interposed a fabric made of long carbon.

The heat treatment is made of two stages: the first one is a solubilization treatment followed by age hardening in order to obtain the T6 state for the alloy. A significant increase in the hardness of the material has been reached. The metallographic characterization did not reveal abnormal grain growth and a significant increase in the grain size of the material, but problems encountered during the sample preparation did not allow us to totally exclude these two phenomena.

For the study of the wear properties, a pin on disk tribometer were used, with a sliding speed of 0.1m/s and a normal load of 1 and 3N. The wear tracks were studied with a profilometer in order to calculate the volume loss and observed with a SEM microscope in order to understand the wear mechanism. The results obtained reveal that the mechanism was oxidative wear in the mild regime. No clear effects of both the reinforcement and the thermal treatments were revealed, so further studies are suggested.

Abstract (Italian version)

Con questo lavoro si vogliono investigare le proprietà di resistenza usura di un materiale composito a matrice metallica (MMC) in cui la matrice è costituita da una lega di alluminio 6005 (contenente silicio e magnesio come principali elementi alleganti) mentre il rinforzo è costituito da fibre di carbonio corte. Il materiale è stato prodotto con la tecnologia del Friction Stir Processing (FSP). Un sandwich costituito da due piatti di alluminio con interposto un tessuto in fibra di carbonio viene lavorato con una macchina fresatrice. Un utensile rotante appositamente progettato viene inserito nel materiale e trascinato all'interno di esso. L'azione dell'utensile permette di rompere il tessuto formando le fibre corte e mescola il metallo in modo da saldare tra loro i due piatti e distribuire all'interno di essi il rinforzo.

Inizialmente è stata eseguita una caratterizzazione microstrutturale per evidenziare l'eventuale presenza di difetti legati alla produzione e per misurare la frazione superficiale del rinforzo e la sua distribuzione all'interno del materiale.

Successivamente è stata effettuata la messa a punto dei trattamenti termici. Per valutarne l'efficacia sono stati effettuati dei test di durezza durante i trattamenti a intervalli di tempo regolari in modo da avere l'evoluzione della proprietà del materiale. Successivamente il materiale è stato analizzato con un SEM per valutare gli effetti della temperatura e del tempo di trattamento sulla microstruttura (dimensione dei grani e precipitati). Dai risultati ottenuti è emerso che il massimo della durezza è ottenuta dopo una solubilizzazione a 540°C per un'ora, seguita da una fase di invecchiamento naturale a temperatura ambiente per una settimana e infine un invecchiamento artificiale a 180°C per 10 ore in modo da ottenere per il materiale lo stato T6. Non sono stati evidenziati fenomeni di ricristallizzazione secondaria (Abnormal Grain Growth).

Il test utilizzato per valutare la resistenza all'usura del composito è il Pin-on-Disk. I parametri utilizzati sono stati una velocità di 0.1m/s e due differenti carichi di 1 e 3N. Con un tribometro è stato possibile misurare l'evoluzione del coefficiente di attrito durante il test. Dalle analisi effettuate sulle tracce formate durante il test è stato poi possibile misurare il volume di materiale asportato dall'usura. I campioni analizzati sono di diversi tipi: senza trattamento termico, con trattamento parziale (solamente l'invecchiamento artificiale) e con il trattamento completo (stato

T6). Sono stati testati sia la lega di alluminio senza rinforzo che il materiale composito. Dai risultati ottenuti non è stato possibile rilevare un chiaro effetto sia del trattamento termico effettuato che della presenza del rinforzo sull'usura del materiale. L'effetto del carico applicato rilevato è stata una riduzione del coefficiente d'attrito e un aumento del volume asportato.

Tramite l'analisi delle micrografie ottenute con il SEM è stato poi possibile individuare il meccanismo di attrito del materiale nelle condizioni testate (velocità e carico applicato). In tutti i campioni è stato individuato uno strato compatto di ossido sulla superficie delle tracce e, al di sotto di esso, uno strato composto da particelle equiassiche di materiale asportato e successivamente sinterizzate dall'effetto del carico e del calore generato dall'attrito. Queste considerazioni portano ad individuare il meccanismo di attrito come ossidativo in un regime di usura dolce. Il meccanismo individuato giustifica lo scarso effetto sia del rinforzo che dei trattamenti termici sull'usura, in quanto la presenza dello strato compatto di ossido va a mascherare il materiale metallico nascondendo gli effetti dei trattamenti.

Innanzitutto vorrei ringraziare le prof. Irene Calliari dell'Università di Padova e Jacqueline Lecomte-Beckers dell'Università di Liegi per avermi dato la possibilità di lavorare a questo progetto e di aver passato questi ultimi mesi a Liegi. Un grosso ringraziamento va anche alla Dr. Anne Mertens per avermi seguito durante tutto il progetto aiutandomi e dandomi numerosi e utilissimi consigli e alla prof. Aude Simar per aver collaborato al progetto.

Ringrazio poi tutto il dipartimento MMS dell'Università di Liegi per avermi accolto e aiutato non solo nella parte tecnica ma anche ad ambientarmi in una nuova città, in particolare Neda Hashemi, Jérôme T. Tchuindjang, Hakan Paydas, Rosine Pirson, Olivier Dedry, Herny-Michel Montrieux, Sylvie Salieri, Sylvie Reginster, Jocelyn Delahaye e Tommaso Maurizi-Enrici.

Voglio inoltre ringraziare tutti i miei amici i quali ho condiviso i momenti migliori e le difficoltà di questi ultimi magnifici anni.

Il mio più grande ringraziamento va poi alla mia famiglia e ai miei genitori senza i quali tutto questo non sarebbe mai stato possibile.

Index

List of Figures

List of Tables

1 Introduction and Objectives

The need for weight reduction of mechanical components, especially in transportation and aerospace applications, is increasing the importance of light alloys such as aluminum, magnesium and titanium thanks to their good mechanical properties and their low densities. Ferrous alloys still have better properties, but light alloys can be improved with the addiction of non-metallic reinforcements to create composites. The main problem in the fabrication of good metallic matrix composites with "liquid" technologies (that involve molten metals) is their high chemical reactivity with the molten metal [49]. For these reasons solid state processes, such as friction stir processing, have been developed. Friction stir processing is a derivation of the friction stir welding technology. In friction stir welding "*a non-consumable rotating tool with a specially designed pin and shoulder is inserted into the abutting edges of sheets or plates to be joined and traversed along the line of joint*." [3] The heat generated by the friction between the tool and the metal surface and the intense stirring of the material allow the creation of the weld. The same principle has been used for the production of MMCs.

The wear properties of a 6005 aluminum alloy with the addiction of short carbon fibers produced by friction stir processing have been studied. In particular a specific thermal treatment has been developed. After that wear tests (pin on disk) were made in order to quantify the wear properties of the material (in particular friction coefficient and volume loss).

The first part of the experiments was the microstructural characterization of the material to reveal the effect of the thermal treatments on the microstructure of the material (in particular the appearance of abnormal grain growth phenomena). The second part of this work is the characterization of the wear mechanism, made by the observation of the wear tracks with a SEM microscope.

2 State of the Art

2.1 Friction Stir Process

Friction stir processing was firstly developed as a welding technique by The Welding Institute (TWI) of UK in 1991 for aluminum alloys[1,2].

Friction stir welding (FSW) is a solid-state joining technique, so there is no fusion of material during the process. The basic concept is very simple: a non-consumable rotating tool, comprising a pin and a shoulder, is inserted into the abutting edges of plates to be joined, and moved along the line of the weld. A representation of the process is given in Fig. 2-1.

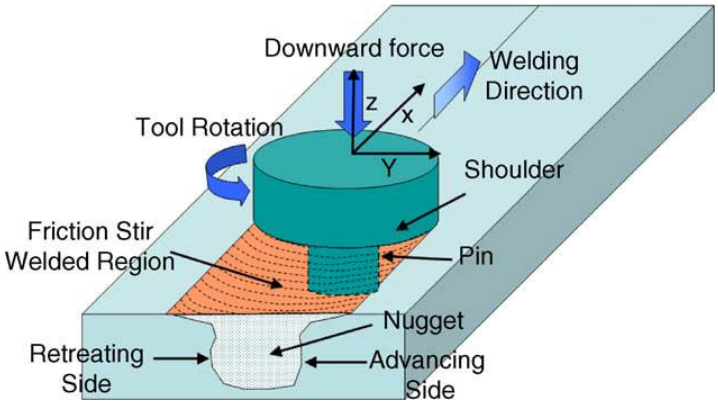

Figure 2-1 Representation of the friction stir welding process. [3]

The tool has two primary functions: generate heat and move material. The heat is generated by the friction between the tool and the plate and also by the high plastic deformation of the material. The heat generated is localized under the tool and softens the metal, making the movement of the material around the pin possible, thanks to the rotation and translation of the tool. The high heat generated and the strong plastic deformation lead to the generation of a fine and equiaxed recrystallized structure [4,5], so the friction stir welds exhibits good mechanical properties.

Nowadays several weld configurations are possible with this technology (see Fig. 2-2).

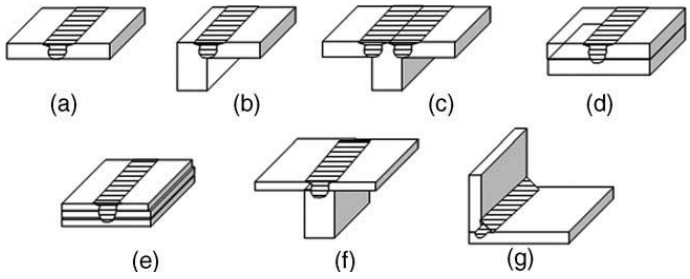

Figure 2-2 Joint configurations for FSW: a) square butt, b) edge butt, c) T butt joint, d) lap joint, e) multiple lap joint, f) T lap joint, g) fillet joint [6].

The optimization of welding parameters is fundamental to obtain a good quality joint without defect.

Tool geometry is the most influential aspect because it governs the material flow and, as a consequence, also the traverse speed at which the welding can be conducted. At the initial stage the heat results primarily from the friction between the pin and the material. When the material is softened enough the pin can be fully inserted and then the major part of the heat is generated by the friction between the shoulder and the surface of the material. So for a correct heat generation, it is necessary to choose the correct shoulder geometry, in particular its diameter. Moreover TWI designed different shoulder's profile to suit different materials and conditions (see Fig. 2-3). The pin, on the other hand, is responsible of plastic deformation and material flow, so its geometry if fundamental to obtains good quality joint. The most common is the cylindrical pin, but different and more complex geometry have also been developed. An important characteristic of the pin is its length that allows to obtain a weld through the whole thickness of the plates.

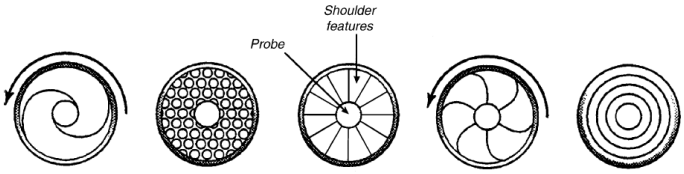

Figure 2-3 Different shoulder's profile developed by TWI. [6]

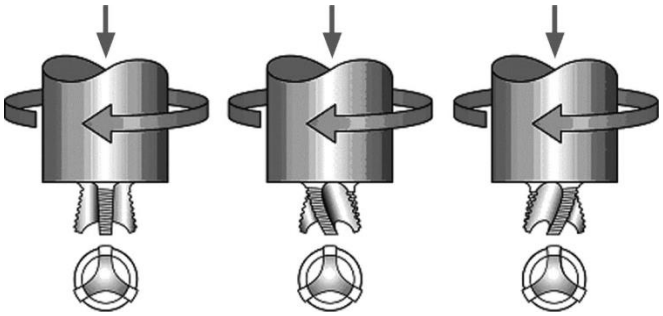

Figure 2-4 Examples of pin's geometry. Flared-Triflute® developed by TWI [7].

The material of the tool have to be chosen wisely, otherwise a strong wear can occur during the process decreasing the quality of the weld.

Friction stir processing is used not only as a welding technique, but it is also used for microstructural modifications. For this reason it is used as a post-production process to obtain superplasticity, to enhance room-temperature formability and to improve the microstructure of casted components by decreasing porosity [54].

2.1.1 Processing parameters

The two main parameters in friction stir welding (and processing) are the tool rotation rate ω (expressed in rpm) and the tool traverse speed v (usually in mm/min). The rotational speed controls the stirring and mixing of the material and the frictional heat developed. So a higher ω results in a more intense stirring and higher temperatures. Also the transverse speed controls the heat input to the material: heating and cooling rate increases as the transverse speed increases. At higher transverse speed the peak temperature reached is lower[8]. It is possible to summarize the effects of ω and v on the heat generated with a single parameter that is the ratio between the rotational speed and the transverse speed. So higher values of this ratio correspond to a higher heat input and "hotter" conditions [9].

In addition to these two speeds, another parameter that influence the quality of the joint is the tool tilt angle with the surface of the workpiece. It ensures that the shoulder holds the material stirred by the pin and moves efficiently the material from the front to the back of the pin.

The choice of the parameters has a strong influence not only on the quality of the weld (defects) but also on the final microstructure and properties of the material[8,9].

2.1.2 Microstructure after friction stir processing

In a friction stir welded joint, different zones with different microstructures and, as a consequence, different mechanical properties can be easily recognized. The differences are mainly due to the different heat input (and temperature distribution) in the various zones and to the magnitude of the plastic deformation.

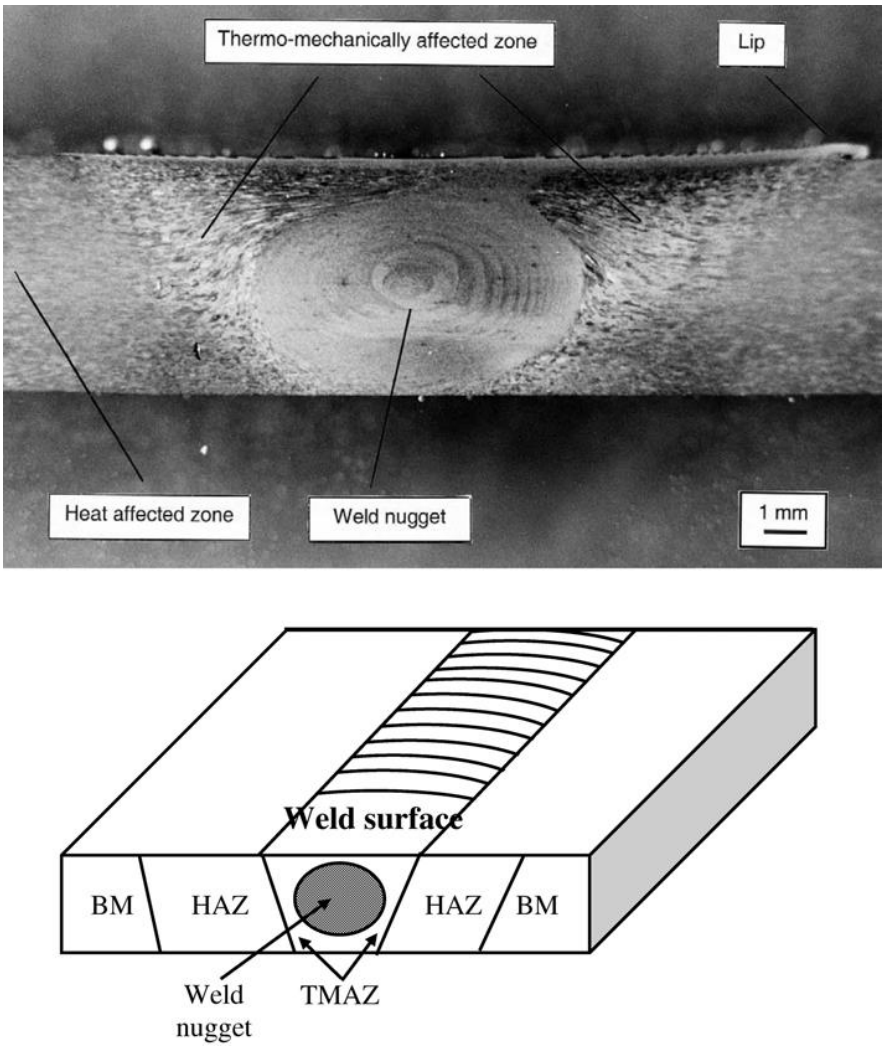

Figure 2-5 Microstructure and schematic representation of a joint produced by FSW [10].

Starting from the center of the weld, there are:

- Nugget zone (NZ): the intense plastic deformation and heating generate a recrystallized fine equiaxed structure. In the interior of the grains, there is usually a low dislocation density[4,11]. Moreover the grains have a high density of sub-boundaries [12] and subgrains[13]. Under particular welding conditions an onion ring structure can develop as in Fig. 2-5. The fine-grained structure is generated by dynamic recrystallization in the nugget zone [7, 14-40]. The influence of processing parameters is very high: decreasing the heat input will generate smaller grains. This can be achieved by reducing the rotational speed with constant transverse speed [19,35,36,41,42] or by decreasing the ratio ω/v[16].
- Thermo-mechanically affected zone (TMAZ): this zone experiences both increase in temperature and deformation, but at a lower level in comparison to the nugget zone [3]. No recrystallization is observed because the deformation is insufficient to start the process. The temperature reached is sufficient to dissolve some precipitates in the TMAZ. [29,43]
- Heat affected zone: this zone experiences the thermal cycle, but no plastic deformation. The grains structure is the same as in the base material, but there is coarsening of the precipitates[9,13].

Several studies reveal the appearance of abnormal grain growth phenomena after high temperature heat treatments in friction stir processing[45-48].

2.1.3 Composite production via friction stir processing

One of the main problem in the production of metal matrix composite by casting route is the deterioration of the reinforcement due to their contact with the molten metal. Moreover other problems are correlated to the wetting behavior of the reinforcement. In particular Carbon fibers have a high reactivity with molten aluminum, making difficult the development of high quality composites [49]. One of the solution adopted to overcome these problems is the coating of the

fibers with metals [50], but this increase the cost of the reinforcement and requires more steps in the production of the material.

In friction stir processing the metals never reach the melting temperature avoiding these problems. The biggest disadvantage of producing composites via FSP is that is impossible to produce long fibers MMC.

Different techniques can be used to insert the reinforcements in FSPed composites: if the reinforcements are in the form of small fibers or particles (such as ceramic particles or carbon nanotubes) they can be placed in holes [51] or grooves [52,53] made on the surface of the workpiece that is later friction stir processed. Another interesting method to produce a short fiber MMC is to put the reinforcement in form of a fabric between two plates of metallic materials and then process the so made sandwich (see Fig. 3-3). The stirring action of the pin ensures both the fragmentation of the reinforcement and the dispersion of the fibers in the matrix. This process has the advantage (in comparison to the others techniques described) that it is adapted for a large-scale production and there is no risk that the holes or the groove leave porosities and defects on the workpiece [54,55].

The optimum welding parameters are different for composites in comparison to the processing of the base material [56]. It is also necessary to obtain a homogeneous distribution of the reinforcement because it has a big influence on the microstructure and on the mechanical properties of the final material. [54] Multiple passes with partial overlapping ensure better results [54]. Moreover the tool wear is very important in the production of MMC due to the abrasion by the hard reinforcement, so specific harder materials are required for the tool [57].

2.1.4 Advantage and limitation of the process

The main advantages are [10]:

- Being a solid state process, problems of hot cracking and porosities are, in principle, avoided
- Low temperatures and the rigid clamping of the workpiece reduce the distortion
- No consumables, such as filler metal or gas, are required
- The process is environmental friendly due to the absence of fumes or UV radiation normally produced with classic welding techniques
- The process can be easily automated
- Welding can be carried out in any position since no molten metal is developed
- Alloys generally classified as unweldable give good joint quality
- Possibility to weld together dissimilar alloys
- Only 2.5% of energy used for laser welding is required [58]
- A fine recrystallized structure is obtained
- Easier production of metal matrix composite (especially with light alloy)

The main limitations are [10]:

- Specific defects (kissing bond and tunnel defects)
- Internal residual stresses for the clamping of the workpiece
- Macroscopic defects at the beginning and at the end of the weld
- High forces required
- Different parameters and tool geometry for different welding conditions

2.2 6000 series aluminum alloys

2.2.1 Microstructure

Nowadays, in view of the necessity of weight reduction especially in the transport field, light alloys such as aluminum, magnesium and titanium are growing in importance, even if steel remains the principal metallic material produced. In particular, what makes light alloys very interesting is their high mechanical properties to density ratio.

Among aluminum alloys, Al-Mg-Si alloys with Cu addition are extensively used thanks to their good mechanical properties, formability and corrosion resistance [111]. Moreover they have an excellent extrusion resistance and they are heat treatable. The main drawback of the 6000 series alloys is that it is difficult to join using fusion welding techniques [3,113]. In this alloy the hardening effect is due to the precipitation of the precursors of the stable precipitates Mg_2Si. Usually chromium and manganese are also added. These two elements have no great effects on the mechanical properties, but control the microstructure of the material[113,114,115]. Cu enhances the hardness and refines the grains, giving benefits on the mechanical properties [116]. It also modifies the precipitation sequence and promotes the precipitation of the Q-phase ($Al_5Cu_2Mg_8Si_6$) [117,118].

The thermal treatment made on this kind of alloy is the age hardening and several conditions are obtained. The most common are:

- T4: solution treatment and natural ageing at room temperature
- T6: solution treatment and then artificially aged (in ovens)
- T5: cooling from elevated temperature shaping process and then artificial ageing
- T78: slightly over-aged material

The precipitation sequence in this alloys is generally described as [119,120] super-saturated solid solution (SSSS) → cluster/GP zones → β'' phase → β'/Q' phase → β/Q phase. Wenchao et al. [121] investigated also the initial stages of the mechanism that leads to the precipitation of the

GP zones. The precipitation mechanism is revealed by DSC analysis as the one reported in Fig. 2-6.

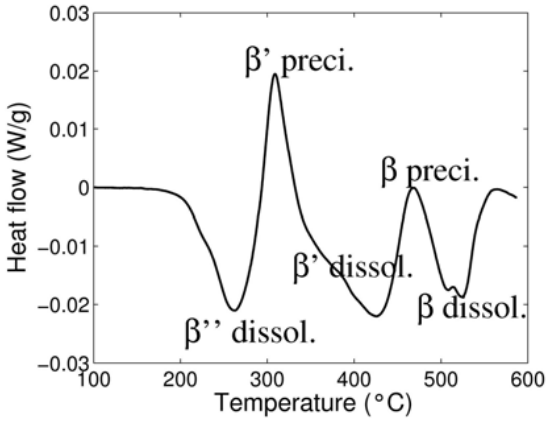

Figure 2-6 DSC of a 6005 aluminum alloy with the same composition of the one used in this project [10].

GP zones are constitute by aggregates of solute atoms fully coherent with the matrix. They serve as nucleation sites for the precipitation of the β'' phase. β'' precipitates are small needle-shaped precipitates (see Fig. 2-7), coherent to the Al matrix along their long axis direction. They provide the most important contribution to the hardening of the material, and they are the most effective obstacle to the movement of the dislocation [121]. *"The existence of a three-dimensional coherency strain-field around the needle-shaped β'' precipitates would be the most notable obstacles for the dislocation movement because it provided larger obstacles in comparison with other phases"* [121].

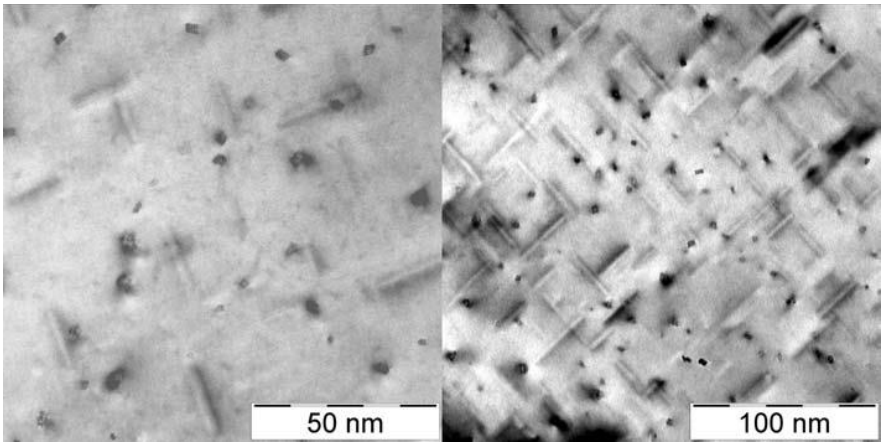

Figure 2-7 β'' precipitation in the base material [10].

The main non-hardening precipitates observed in 6005 alloy can be divided in four categories: β(Mg_2Si) phase, iron rich, silicon precipitates and dispersoïds which are rich in chromium and manganese [10]. Coarse β phase is the final stable phase obtained following the precipitation mechanism. It does not make a significant contribution to the hardness of the alloy. The bigger β precipitates are not dissolved during homogenization treatments. The excess of silicon usually present in these alloys allows the precipitation of silicon rich particles after the precipitation of the stable β phase. Intermetallics are Al-Fe, Al-Fe-Si and Al-Fe-Mn-Si, the most common being the α phase(AlFeMnSi). They are iron rich particles with a typical size of 1-10μm.Dispersoïds are small iron rich precipitates with a typical dimension of 100nm. The difference with the intermetallics are the lower dimensions and the higher manganese content.

2.2.2 Thermal treatments

The 6005 alloy can be naturally aged at room temperature, leading to a significant increase in hardness as reported in Fig. 2-8. The process is complete in less than one year [10]. The results are strongly influenced by the exact alloy composition and, in particular the Cu content. This process occurs only starting from a super saturated solid solution condition (higher is the concentration of the solution and more efficient is the precipitation) so a solution treatment followed by water quenching is highly suggested [10,44,58,93].

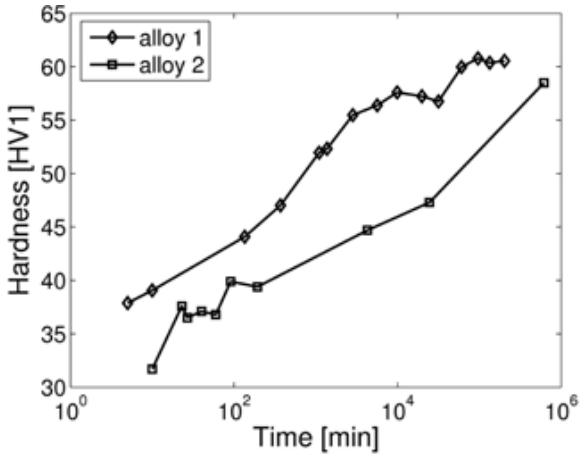

Figure 2-8 Natural ageing effect on hardness on two different 6005 alloys after solution heat treatment [10].

The temperature of the solution treatment generally varies with the composition of the alloy. For alloy 6005, the kinetic of the ageing treatments (and as a result the hardness of the material) is independent from the temperature used [44]. The peak strength for this alloy is reached for the T6 state, so after artificial ageing at higher temperatures (around 180°C). For reaching the higher properties in a shorter time, it is suggested to carry the artificial ageing after a few days of natural ageing, in order to have a sufficient number of GP zones [10]. The results obtained are strictly correlated with the volume fraction of the β'' phase inside the material. The optimal size and number of hardening precipitates is obtained for 6-10 hours of age hardening. For longer times the β'' precipitates dissolve and the precipitation of non-hardening phases begins. As a consequence the properties of the material decrease [10] (see Fig. 2-9 and also section 4.2). This condition is called over-ageing and can be useful for having better corrosion properties in alloys with high Cu contents.

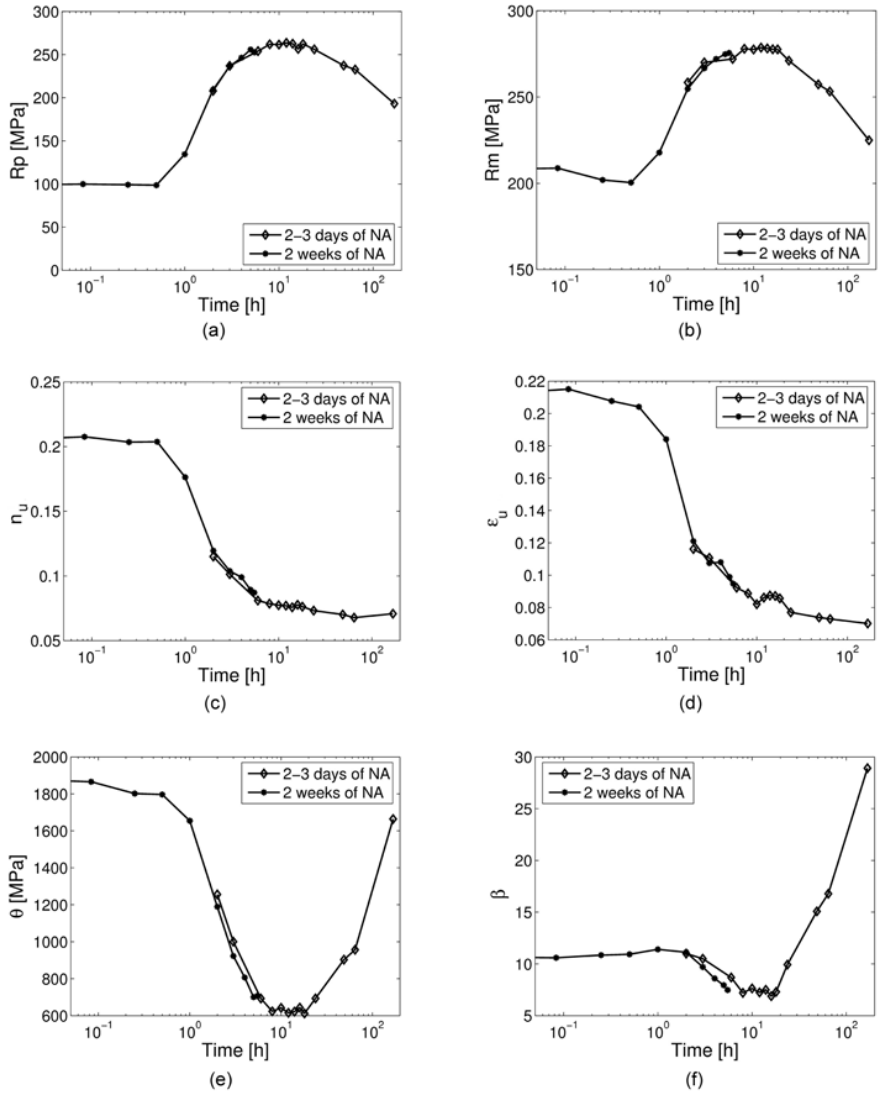

Figure 2-9 Evolution of the tensile properties with the ageing time [10].

2.3 Wear

Wear is the progressive loss of material during relative motion between a surface and contacting substance or substances. It is a very important phenomena from the technological point of view, because wear can be a big problem. The loss of material and the degradations of the surfaces of components can lead to an incorrect operation of the machines, making necessary interventions to correct the defect or, in the worst case, the substitution of the damaged piece.

There are different wear mechanisms that lead to different kinds of wear:

- Adhesive wear, when a normal load is applied between two sliding surfaces. The local pressure at the asperities always present on the surface can reach an extremely high value due to the small contact area. The pressure can exceed the yield stress of the material. Then the asperities are deformed by plastic deformation increasing the contact area. As a consequence strong adhesive junction may be formed, and the relative motions of the surfaces shear them causing the damaging of the surface. This process is also enhanced by the increase in the temperature on the surface that lowers the yield strength.
- Abrasive wear happens when a hard rough surface slide against a softer one.
- Corrosive wear occurs when there are chemical reactions between the two materials involved or between one material and the environment. As a consequence reaction products develop on the asperities changing the surface properties. During sliding, the wear of these products that can cause crack formations or abrasive wear. This can also lead to the damaging of the surface due to the removal of the reaction products through physical interactions. Also in this case, the increase in temperature enhances the phenomenon.
- Fatigue wear is due to the application of a cyclic loading to the surfaces.

Friction is the resistance an object encounters in moving over another. An important parameter of wear is the friction coefficient, defined as the ratio between the force of friction *(F)* and the normal load applied *(P)*.

$$\mu = \frac{F}{P}$$

The most important parameters that rule wear are: the normal load, the relative speed between the two surfaces (sliding speed), the sliding distance, the materials involved and the environment.

During wear of aluminum alloys it is possible to notice the creation of a layer on the surface called *tribo-layer*. It is a hard layer made of compacted aluminum oxides and other intermetallic phases due to the alloying elements. In the case of wear between aluminum alloys and steel, iron-aluminum intermetallic phases and iron oxides [59-62]. Tribo-layers have an enormous importance in wear. In fact they can protect the bulk material thanks to their higher hardness. However, they also have a negative aspect that is the scuffing damage on the counter-face material.

Riahi et. al. [64] introduce three different regimes of wear, in relations to what happens to the tribo-layer and to the parameters used for the wear tests. Two different regimes are observed: mild wear at low speeds and loads and severe wear for higher values. Zang and Alpas [63] also introduce a third regime for metal matrix composite: the ultra-mild regime, due to the load supporting effect of the reinforcing particles at very low load.

The transition between mild and severe wear coincided with the removal of the tribo-layer [64]. Zhang and Alpas [63] and later Riahi and Alpas [64] studied the influence of the wear parameters (load and sliding speed) on the transition between the two regimes for an aluminum alloy and for aluminum metal matrix composite respectively, making wear maps.

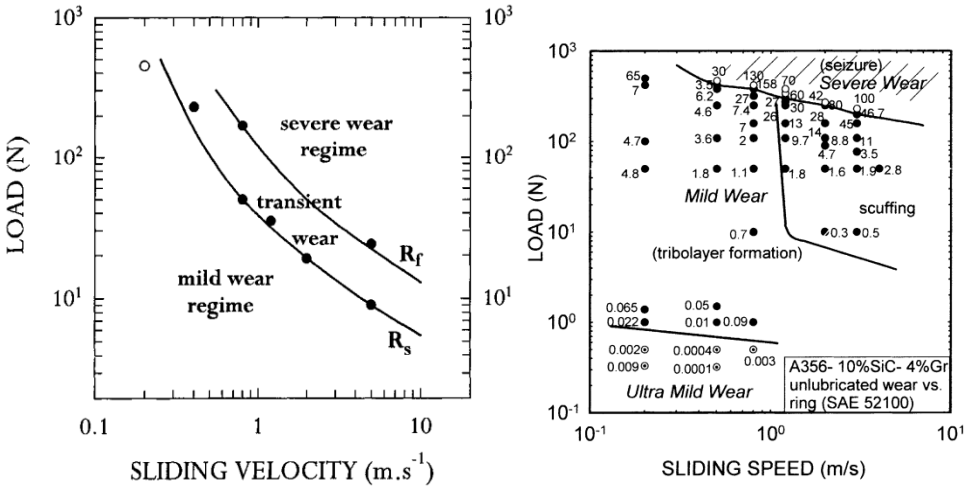

Figure 2-10 Wear maps. On the left wear transition map for 6061 Al against SAE 52100 steel counter face. R_s indicates load and sliding speed at which mild to severe wear transition is first observed CIT. On the right wear map for A356 Al-10% SiC-4% Gr composite worn against SAE 52100 steel counter face [64].

Zhang and Alpas [63] propose a critical temperature criterion for the explanation of the transition between the two regimes. They observed that the transition for the 6061 alloy appears when the bulk temperature of the material reach 395 K. Then they correlate the bulk temperature of the material with the wear parameters, finding that the bulk temperature is proportional to the friction coefficient, to the normal load and to the sliding velocity. At this temperature thermally activated deformation processes are expected to become active and lead to the softening of the material as proposed by Ling and Saibel [65], who postulated that severe wear occurs when the contact surface temperature reaches the recrystallization temperature of the material. So the T_c is defined as the threshold temperature above which thermally activated deformation processes start to control the wear mechanism [63].

Reducing wear is fundamental in all applications. In order to do this two solutions are available: the use of a lubricant or the development of materials with low coefficient of friction and wear rate called self-lubricant materials. The production of self-lubricant material can be achieved by applying coatings (like DLC [66]) or by embedding solid lubricant such as graphite or molybdenum disulfide [67,68]. Coatings ensure the protection of the material only if they are not damaged or communed, instead composites ensure the properties in any situation. Moreover composites show good tribological properties accompanied by good corrosion resistance and higher fatigue life. With hybrid composite, obtained with two kind of reinforcement (for example a hard ceramic material such as SiC and a solid lubricant such as graphite) it is also possible to

associate the lubricant effect with the improvement of the mechanical properties of the alloy [69]. For this reason, MMCs gain a high popularity.

Three important factors determine the performances of MMCs [8]:

1. Intrinsic material factors such as type of reinforcement, particle's size and volume fraction, shape of the reinforcement and microstructure of the matrix
2. Mechanical factors such as normal load, sliding velocity and sliding distance
3. Physical factors such as temperature and environmental conditions

The volume fraction of the reinforcement has a strong effect on the tribology of the material [71-79] and this is mainly due to the improvement of the mechanical properties of the alloy considered [80]. The increase in the volume fraction of the reinforcement involves an increase in the wear resistance of the material, due to the enhancement of the mechanical properties. [80] It has been shown that the effect of the volume fraction is effective above the 20%. Over this critical value there are no important improvements as can be seen from Fig. 2-2. However, if the reinforcement is made by hard particles, the particles can sometimes be removed from the matrix during the wear test and consequently act as an abrasive material, thus increasing the wear rate.

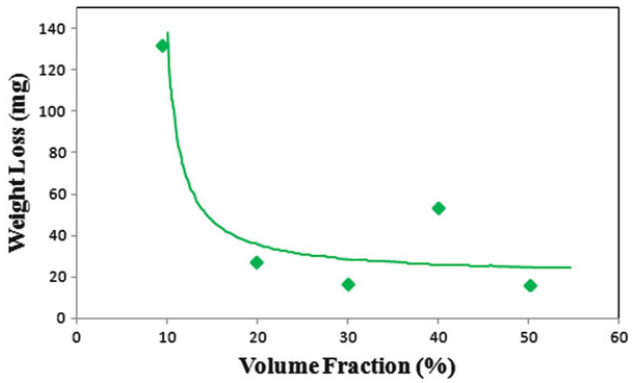

Figure 2-11 Weight loss of an aluminum alloy reinforced with micrometric SiC particles [81].

Also in hybrid composites the increase in the volume fraction of the reinforcements is associated with an increase of tribological properties of the material [82-83].

Another material's parameter that strongly influence the tribological properties is the size of the reinforcement. It is well known that nano-composites show better resistance, but also in the micrometric scale there are important differences in wear rate and coefficient of friction associated with the particle size. However, the effect of particle size on micro-composite is not

clear. Some studies [72] made on a 2014 Al alloy reinforced with SiC showed a superior wear resistance for 15.8µm particles in comparison to 2.4µm. Other researches show an increase in wear rate by increasing the dimension of the reinforcement [84,85]. Moreover a critical particle size has been identified in other works. [85,86] If we compare micrometric with nanometric reinforcements we can see that there is a significant drop in wear rate and friction coefficient with particle smaller than 1µm [87].

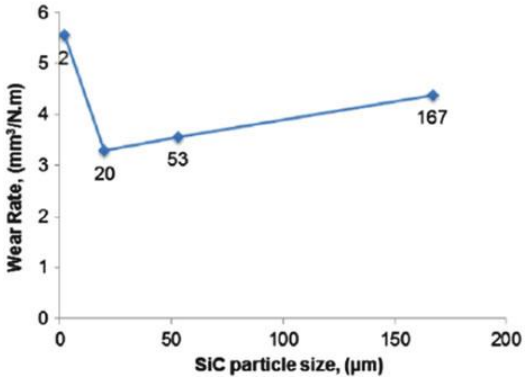

Figure 2-12 Effect of SiC particle size in wear rate of an aluminum alloy [86].

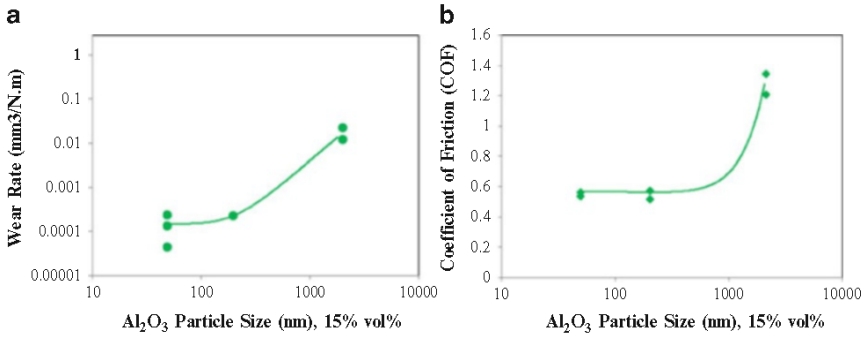

Figure 2-13 Effect of particle size on wear rate and friction coefficient of an aluminum alloy reinforced with 15% of alumina particles [87].

Also the shape and the orientation of the reinforcement have influence on wear resistance. [88] notice that a 3D random distribution of fibers is better than a 2D distribution because the load transfer effect is enhanced. Moreover graphite fibers leads to a stronger improvement of wear resistance in comparison to graphite flakes [89].

Another very important parameter that greatly influences the wear resistance of a material is the applied normal load. Many studies show that an increase in normal load causes an increase in wear rate of the material [50,84,90-98]. High load can break the reinforcement leading to a reduction of mechanical properties. Increasing the normal load lead to an increase of the temperature, that can reach the recrystallization temperature of the material. As a consequence the wear regime changes from mild wear to severe wear, with a significant increase in the wear rate. High load can also cause plastic deformation in the matrix that leads to an increase in the wear rate and to microstructural modifications in the tribo-layer [50]. Also the frictional force increases with the normal load. From Fig. 2-5 it is also possible to notice that a higher volume fraction of the reinforcement lead to a lower effect of the normal load.

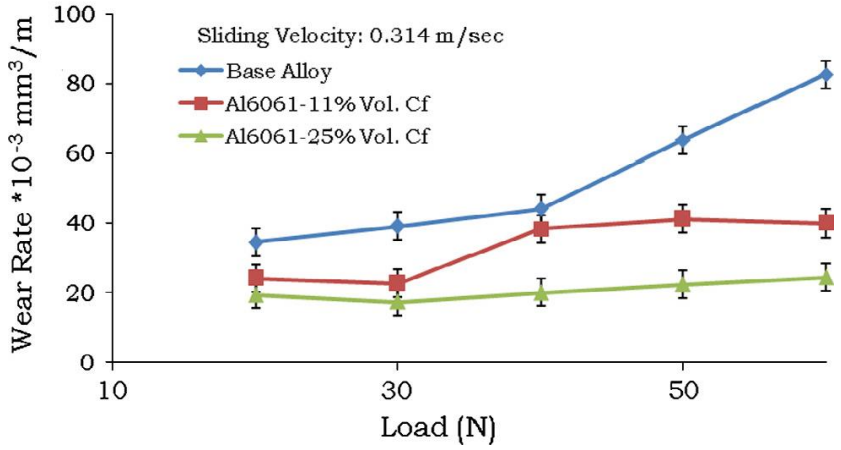

Figure 2-14 Influence of normal load on wear rate on a composite made by Al6061-carbon fibers [50].

At low normal load, some researches show that the wear rate of the matrix without reinforcement and of the composite materials are comparable [91,99]. The effect of normal load on the friction coefficient is different in comparison to wear rate. In fact an increase in the force leads to a reduction of the friction coefficient, as can be seen in Fig. 2-4 [50,77,91,92,97,100,101].

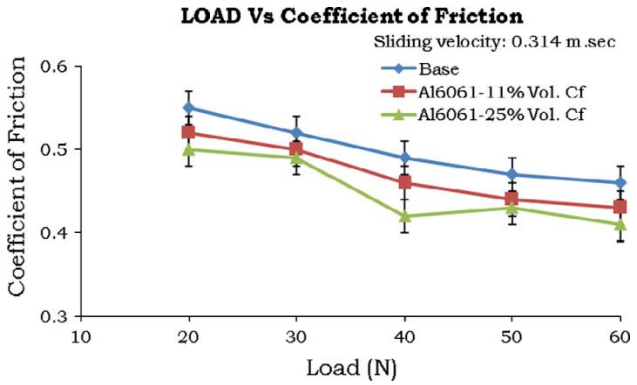

Figure 2-15 Effect of friction coefficient with applied normal load on Al6061-carbon fibers MMC [50].

Ramesh et al. [50] supposed that increasing the normal load results in a greater extent of squeezing out of carbon fibers onto mating surfaces, obtaining a better effect of the solid lubricant. Increasing the normal load also leads to strain hardening of the matrix and thus to better mechanical properties.

The effect of sliding speed on wear rate and friction coefficient is similar. An increase of this parameter causes an increase in the wear rate and a decrease in wear resistance [91,93,98,102]. The variation is usually linear [103,104].

The main effect of sliding speed is the increase of the temperature of the material, leading to softening of the matrix, enhancing of the oxidation and at high speed damaging of the tribo-layer and consequently changing of the wear regime.

In an aluminum alloy without reinforcement at low speed there is an initial decreasing of wear rate and, after a critical value, a rapid increase. This is due to the competition between strain hardening at low speed and thermal softening at higher velocities [63].

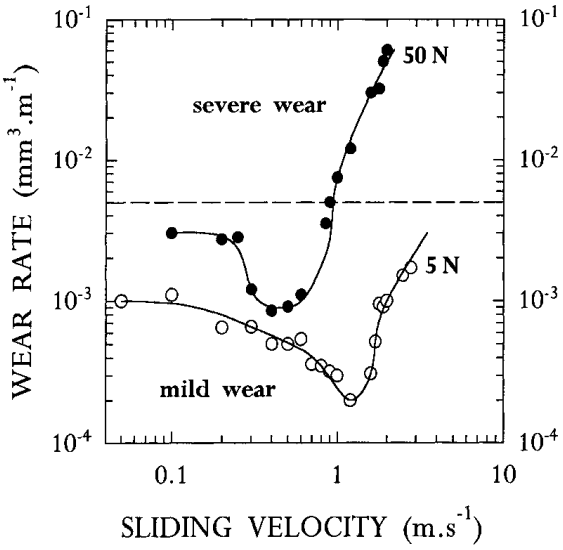

Figure 2-16 Effect of sliding speed on wear rate for a non-reinforced aluminum alloy [63].

Instead, Ramesh et al. [50] working with lower sliding speeds on composite material found a more linear relation. It is also possible to notice in Fig. 2-8 the differences between the composite and the base alloy.

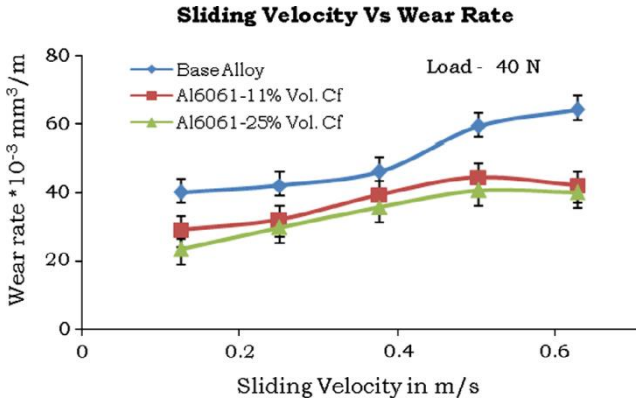

Figure 2-17 Effect of sliding speed on wear rate for Al6061-carbon fibers MMC [50].

Also the effect of sliding speed on the coefficient of friction is similar in comparison to the effect of normal load. In fact it is possible to notice a decrease of the coefficient of friction with sliding speed [50,90-92,101,105,106].

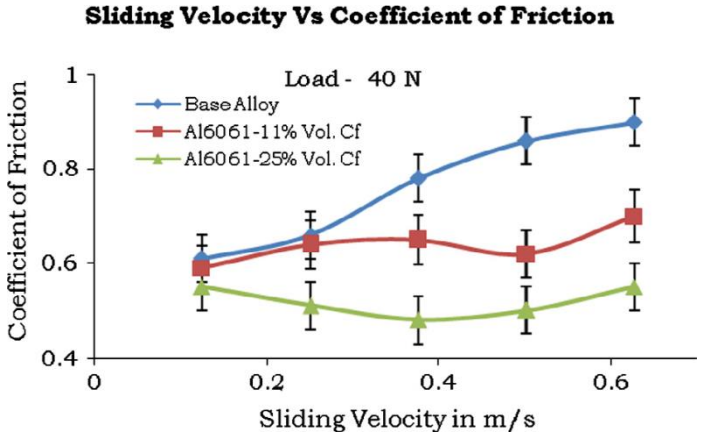

Figure 2-18 Effect of sliding speed on the friction coefficient [50].

3 Experimental Methods

In this chapter, we will descirbe first the base material, the samples production by friction stir process and the thermal treatments (section 3.1). Section 3.2 will describe the characterization method and the techniques used for the interpretation of the results.

3.1 Samples Production

3.1.1 Base Materials

The samples used in this project have been made at the Université Catholique de Louvain (UCL) by prof. Aude Simar, using friction stir processing (FSP).

3.1.1.1 Aluminum Alloy

The aluminum alloy used is 6005A given in the T6 conditions. The main alloying elements are magnesium and silicon. The chemical composition was studied at UCL and the results are summarized in table 1-1.

Alloying Elements	Al	Si	Mg	Fe	Mn	Cu	Cr	Ti	Zn
6005A-T6	98.18	0.81	0.48	0.24	0.11	0.09	<0.01	0.02	0.07

Table 3-1 Chemical composition of the 6005A alloy [10].

The alloy has been given as extruded plates by SAPA RC Profile.

The tensile properties of the alloy in the as-given state are the following:

Direction of loading	Extrusion	Transverse long
Yeld strength at 0.2%, R_p [MPa]	265.5 ± 2.2	255.5 ± 0.7
Tensile strength, R_m [MPa]	287.8 ± 1.2	276.8 ± 0.7
True strain at onset of necking, ε_u	0.086 ± 0.001	0.078 ± 0.02
Strain hardening exponent, n_u	0.085 ± 0.002	0.081 ± 0.003
True fracture strain, ε_f	0.20 ± 0.04	0.18 ± 0.01

Dislocation storage rate, θ [MPa]	918 ± 29	806 ± 4
Recovery rate, β	11.8 ± 0.4	10.1 ± 0.3

Table 3-2 Tensile properties of the 6005A-T6 alloy in the extrusion direction and in the transverse long direction [10].

3.1.1.2 Carbon Fibers

The reinforcement used in the composite are T300 carbon fibers produced by Toray Carbon Fibers America, Inc. This kind of fibers are produced from Polyacrylonitrile (PAN) after thermal treatments at high temperature in controlled atmosphere. They were given as a fabric with the fibers crossed at angles of +45° and -45° without sizing.

The main properties of the fibers are given in table 1-3:

Property	Value
Tensile strength [MPa]	3530
Tensile modulus [GPa]	230
Strain	1.5%
Density [g/cm^3]	1.76
Filament diameter [μm]	7
CTE [$\alpha \cdot 10^{-5}$/°C]	-0.41
Specific heat [Cal/g·°C]	0.19
Thermal conductivity [Cal/cm·s·°C]	0.025

Table 3-3 Properties of the T300 carbon fibers. The data has been taken from the technical data sheet given by Toray®.

3.1.2 Friction stir processing

Both the composite and the reference material (i.e. without reinforcement) are produced by friction stir processing.

The tool used has a cylindrical pin with a diameter of 6mm and a height of 3.6mm. The shoulder of the tool had a diameter of 20mm. These parameters are very important because they have a big influence on the final properties of the material [8].

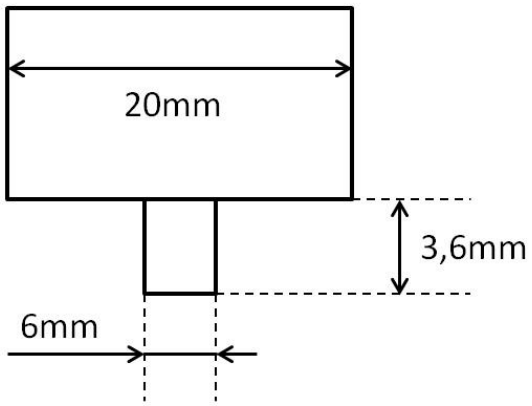

Figure 3-1 Tool's geometry.

Multiple passes have been made in order to obtain a better homogeneity of the material and to increase the width of the welded zone. The distance between each pass was 2mm for a total of 9 passes.

For producing the composite a carbon fibers fabric has been put between two plates of aluminum alloy. The upper plate had a thickness of 2mm and the lower one a thickness of 6mm. This sandwich has been firmly clamped and then friction stir processed.

It was also interesting to compare the composite material and the matrix without reinforcement. When the process begins, the tool breaks the carbon fibers and stirs the material in order to create the metal-matrix composite. To make the reference material, aluminum plates with a thickness of 6mm have been friction stir processed with the same parameters as used for the composite.

The first attempt was made with a rotational speed ω = 1000rpm and a tool's advancing speed in the x direction v = 500mm/min. The result was a inhomogeneous material with defects. For that reason the parameters were changed to ω = 1000rpm and v = 200mm/min. With the new parameters a material more homogeneous and with less defects has been obtained.

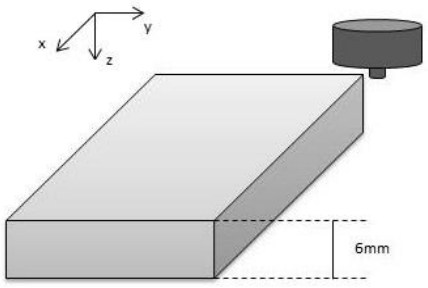

Figure 3-2 Representation on the friction stir process for the production of the reference material.

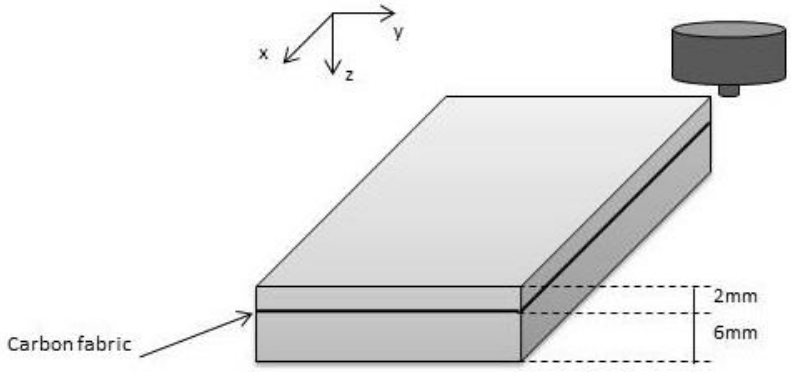

Figure 3-3 Representation of the friction stir process for the production of the composite material.

After that procedure the friction stir processed plates have been cut in order to make the samples for microstructural analysis and wear tests. The external parts in the x direction have been removed due to the presence of the tool marks and due to the fact that the process is not stable. In fact at the beginning and at the end the tool speed is not constant and this creates defects and inhomogeneities in the material.

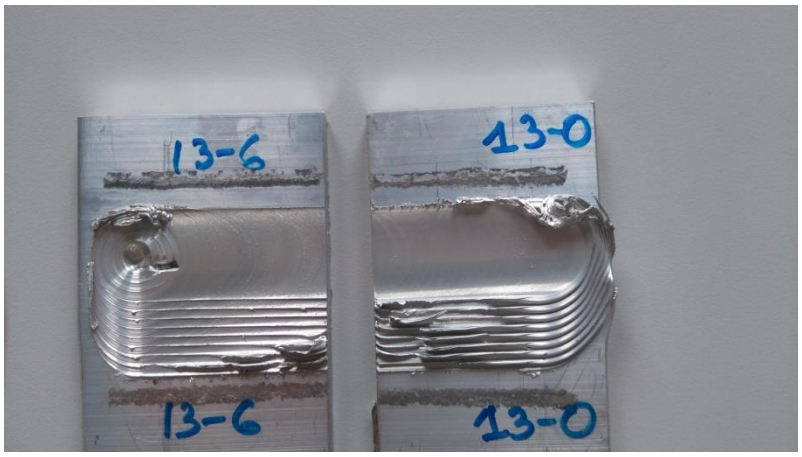

Figure 3-4 Tool marks at the end (on the left) and at the beginning (on the right) of the friction stir processed plate. It is also possible to see the marks left by the clamping system.

Several aluminum plates were friction stir processed with or without fibers to obtain several samples. The samples were called with two number: the first one indicating the processed plate and the second indicating the position inside the weld as presented in Fig. 1-5. In particular samples with 8, 9 and 10 as first number are made with composite material, meanwhile samples with 11, 12, 13 and 14 as first number are without reinforcement. So, for example, sample 8-4 is composite material taken from position 4 in Fig. 3-5.

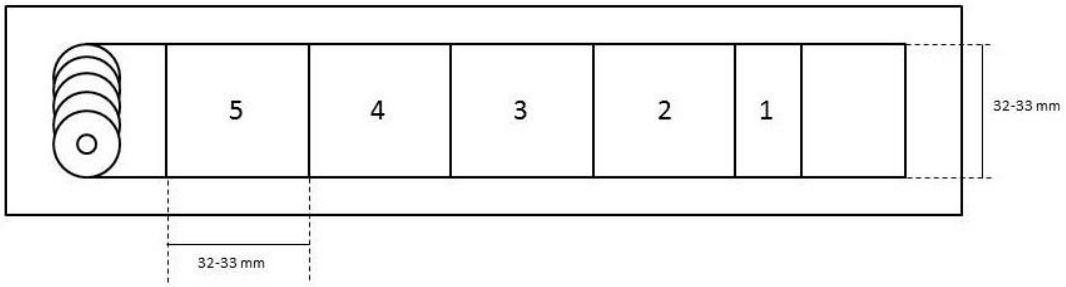

Figure 3-5 Cutting scheme and numeration of the samples. Sample 1 has been used for optical analysis, and the others for the pin on disk test. The external parts have been removed.

3.1.3 Thermal treatments

Thermal treatments are made in order to increase the wear resistance of the composite material. The aim was to increase the hardness of the material.

The thermal treatments consist in two steps: the first is a solubilization treatment and the second one is the age hardening. The solubilization treatment has been made to dissolve all the precipitates present in the material in order to make the alloying elements available for subsequent controlled precipitation during the age hardening. The treatments were made at 540°C as suggested in literature [10,44,58,93] in a Bouvier Technofour® electrical furnace with a power of 12kW. The samples were treated for different times in order to find the optimal parameters. The durations of the solubilization were 0, 1, 2 and 4 hours. The samples were then quenched in water to obtain a final higher hardness [58,93]. In fact the fast cooling avoid the precipitation of intermetallic compounds during this stage, ensuring a better result of the age hardening.

After the solubilization the samples were left for a week at room temperature in order to allow for the precipitation of the GP zones, that in this material act as a precursor for the formation of the hardening intermetallic compounds such as the β'' phase and the stable β(Mg_2Si) phase [119,120].

The age hardening was carried out at 180°C as suggested in literature [10]. The furnace used for the solution treatment could not ensure a good control in this range of temperature, so it has been decided to use a Binder FD056® electrical oven with a power of 1.1kW that ensure more precision in the control of the temperature. To monitor the evolution of the material during the treatment, hardness tests have been carried out after 0, 2, 8, 12, 18, 24 and 48 hours and also observation with ESEM to see the evolution of the precipitates.

The treatment that results in the higher hardness was chosen for the samples used in the wear tests. The best results were obtained with 1 and 2 hours of solution treatment and 10 hours of age hardening. The shortest solution time has been chosen, in order to have a quicker preparation.

The characteristics of the sample used for the wear tests are summarized in the following table (Tab. 3-4).

Sample	Carbon Fiber	Solution treatment	Age Hardening
9-4	X		X
9-5	X		X
10-2	X		
10-3	X		
10-4	X	X	X
10-5	X	X	X
12-3		X	X
12-5		X	X
13-3			X
13-5			X
14-2			
14-3			

Table 3-4 Properties of the samples used for wear tests.

3.2 Analysis

3.2.1 Optical Analysis

The optical observations were made to look at the grain size of the material, to reveal the presence of defects due to the processing and to measure the concentration of the fiber inside the composite.

The first step is the samples preparation: at first the samples were cut then embedded in a hot mounting phenolic resin using a Struers CitoPress 1® machine. The temperature used for the melting of the resin was 180°C. This is quite high for an aluminum alloy (it is the same used for the age hardening), but the short processing time (5 minutes) avoids the appearance of microstructural modifications in the material.

After embedding, the samples have been polished using a Struers Tegramin-30® polisher, first with SiC papers with a mesh from 800 to 1200 and after that with a diamond suspension in water with a particle diameter from 9 to 1μm on a cloth, in order to obtain a mirror polished surface. An alumina suspension has not been used to avoid the risk of the oxidation of the samples. The polishing process was quite delicate due to the low hardness of the aluminum alloy and the presence of small hard particles (the carbon fibers) that easily scratch the surface.

For the evaluation of the grain size, it was first necessary to highlight the grain boundaries. This can be made by etching the surface of the sample with the proper etchant. The choice of the etchant solution has to be done in relation to the base material and to the feature that needs to be observed (i.e. grain boundaries, intermetallic particles, etc.).

Different etchant were tested before obtaining good results. The first solution tested was the Keller's reagent made with 2ml HF (48%), 3ml HCl (conc.), 5ml HNO_3 (conc.) in 190ml of H_2O at room temperature [123]. The result was not good because the solution tends to corrode uniformly all the surface without highlighting the grain boundaries as reported in Fig. 3-6.

Figure 3-6 Effect of the etching with the Keller's reagent. The sample were uniformly corroded without highlighting the grain boundaries.

The second etchant that has been tried was 10ml HCl (conc.), 30ml HNO_3 (conc.), 5g $FeCl_3$ in 20ml of H_2O [123], but the results were the same as for the previous solution.

Better results were obtained with an aqueous solution with 5% of HF (conc.) [10,44] at room temperature. After 3.5 minutes of immersion the grain boundaries started to be highlighted but not clearly. Increasing the immersion time led to a uniform corrosion of all the surface. For that reason it was possible to have only an idea of the average grain size.

For the composite materials this etchant turned out to be too aggressive, leading to a severe corrosion of the material (see Fig. 3-7). This was due to the enhancement of the corrosion caused by the carbon fibers. For that reason a more diluted solution has been tried. The samples were etched with an aqueous solution with 0.125% HF (conc.) at room temperature for more than 3 minutes. In this case the results were quite good especially for the solution treated samples. The grain boundaries were clearly highlighted, but only in small number in localized spots as reported in Fig. 3-8.

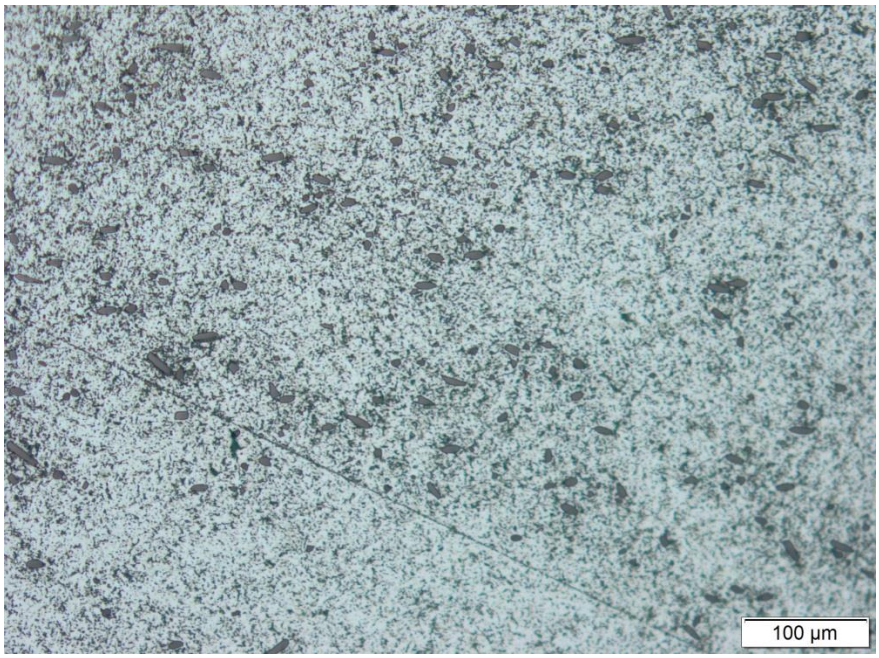

Figure 3-7 Etching test on the composite material with a 0.5% HF (conc.) aqueous solution at room temperature for 20 seconds.

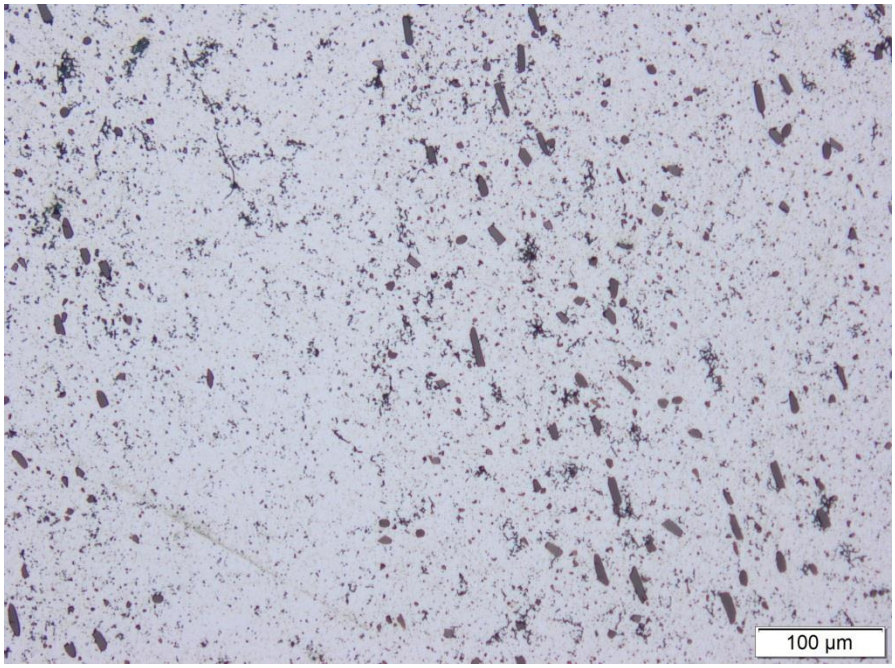

Figure 3-8 Composite samples after the etching with a 0.125% HF (conc.) aqueous solution at room temperature for 3.5 minutes.

After the etching the samples have been observed with an Olympus BX60M® microscope at different magnifications. The pictures taken with the optical microscope were elaborated with the software ImageJ® (Fig. 3-9) to calculate the surface fraction of the fibers inside the composite

material. After the image processing the software gives the value of the surface fraction of the reinforcement.

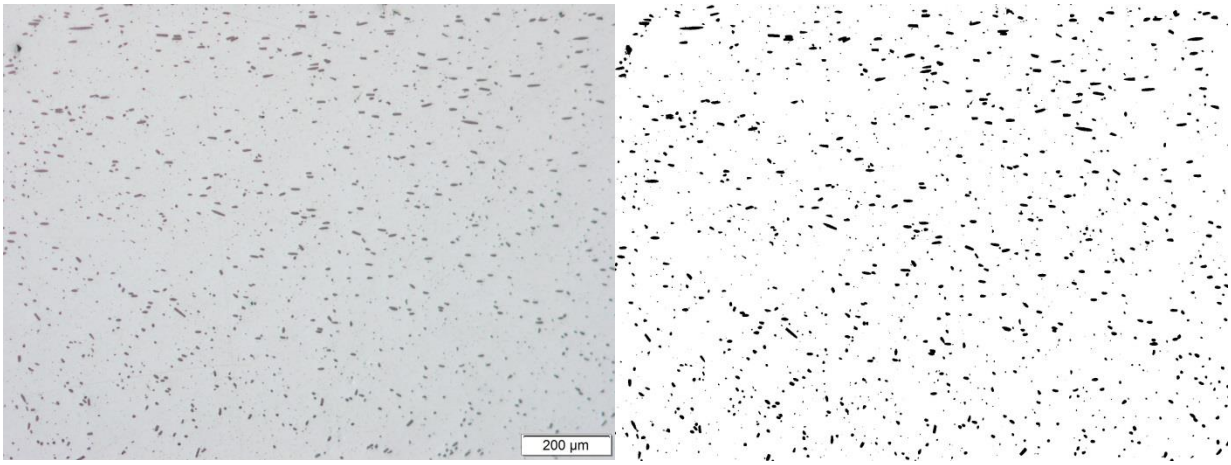

Figure 3-9 Example of the image processing to evaluate the fiber's surface fraction inside the composite material.

3.2.2 SEM Analysis

Observations were also made with an ESEM in order to obtain better results in the measurement of the grain size, to study the precipitation of intermetallic compounds during the thermal treatment and to study the wear mechanism observing the wear track made with the pin on disk test.

For the evaluation of the grain size and for the evaluation of the treatment's effects, the sample preparation was similar to the one used for the optical analysis. The samples were embedded, mirror polished and then etched following the same procedure. In this case the resin used was a bit different: it was a phenolic resin made conductive with the addition of a carbon filler. The conductivity of the resin is required to avoid the accumulation of electrical charges on the sample during the observation. After etching the samples were mounted on a specifically designed support using a conductive adhesive also containing carbon. Moreover two tracks were painted with a silver painting to enhance the evacuation of electrical charges during the analysis. The preparation of the samples for studying the precipitates after the thermal treatments was the same, but without the etching procedure.

The samples were studied at different age hardening time in order to obtain information on the evolution of the precipitates and of the microstructure, in particular grain size, of the material. Moreover Energy-Dispersive X-ray Spectroscopy (EDS) analysis were made on the precipitates for their chemical characterization. Secondary electrons were used for the direct observation.

3.2.3 Hardness Test

Hardness tests were made because they allow to evaluate the effectiveness of the thermal treatment with a simple and fast test. The hardness measurements were made during the age hardening after 0, 2, 8, 12, 18, 24 and 48 hour to monitor the evolution of the material.

Due to the relatively low hardness of the material, a HV1 test has been chosen, so a Vickers test with a normal load of 1kg with a Emco Test M1C 010® durometer. The hardness has been measured as the average value for ten different points in each sample.

3.2.4 Pin on Disk test

The pin on disk has been the main test used in this project. It allows to obtain the wear parameters such as the friction coefficient, the volume lost during the process and also to understand the wear mechanism thanks to the SEM analysis made on the track developed during the test.

The configuration of the tribometer is very simple (see Fig. 3-10): a pin is pressed against a rotating disk by a normal load. The disk rotates with a constant speed thanks to an electrical engine (see, e.g., Gee, 1993, ASTM and ASME, 1997). It is also possible to make the test at different temperatures thanks to an oven present in the apparatus.

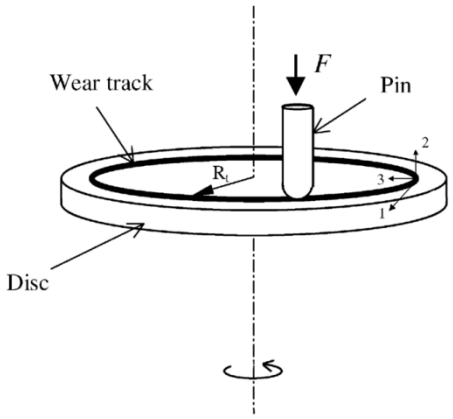

Figure 3-10 Schematic representation of the pin on disk apparatus [122].

There are two possible configurations for the test: in the first one the pin is made of the material to be tested and the disk is made of an hard or abrasive material. Instead in the second configuration the disk is made of the material to be tested and the pin is usually made by an harder material. In our experiment the rotating part was the sample and the pin was a 100Cr6 steel ball with a radius of 6mm.

Two tracks were made on each of the twelve samples (see Fig. 3-11): the first one with a radius of 8mm and a normal load of 1N and the second one with a radius of 10mm and a normal load of 3N, in order to discover if there are changes in the wear mechanism in relation to the load.

It is very important that the samples during the test are firmly clamped in order to avoid vibrations that can distort the results of the test.

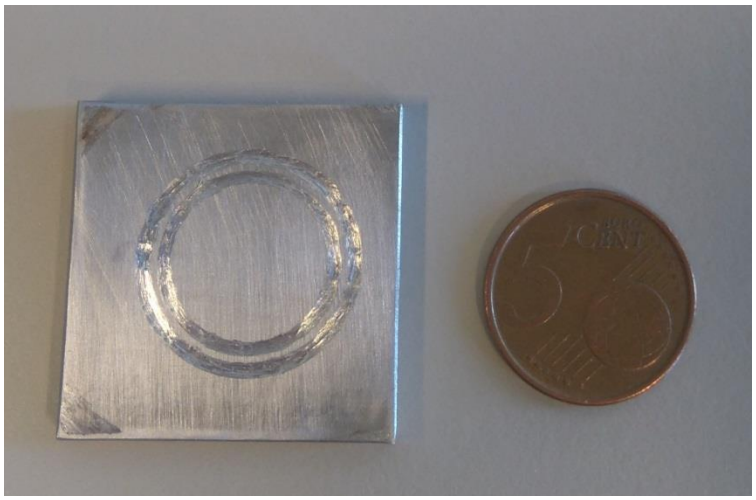

Figure 3-11 Sample after the pin on disk test. The two wear tracks are clearly visible.

The parameters used during the test were a sliding distance of 500m and a rotating speed of 0.1m/s. The rotating speed and the normal load have been set to low values in order to reduce the heating of the samples during the test. All the tests have been carried out at room temperature and without lubricant. The samples and the pin were simply cleaned with ethanol.

During the test the machine gives the real time evolution of the friction coefficient and the depth of the track. The other parameters have been calculated with further analysis.

3.2.5 Profilometer analysis

The profilometer has been used to create a mapping of the wear track, in order to calculate the volume lost during the test.

Usually, when the tracks are very uniform, only four points are required to describe the wear process. In our case the tracks were inhomogeneous due to the presence of some clusters of broken oxide developed during the pin on disk test. In this situation the best choice is to map the whole track, but this required too much time. In order to have representative data but without spending too much time for the analysis, four segments have been mapped for each track. The

length of the segments have been chosen in order to reduce the local perturbation caused by the oxide cluster.

Subsequently the profile of the segments were elaborated with the Vision® software and the numerical data were elaborated with Excel® in order to calculate the volume lost during the wear test. In order to do that the average profile of the segment has been integrated over the segment's length. With the data obtained from the mapping, the volume loss was calculated. From this value then the wear coefficient has been obtained dividing the volume loss for the total length of the track (500m).

3.2.6 SEM observations of the wear tracks

Also the wear track made during the pin on disk test were studied with the SEM in order to obtain more information on the wear mechanism. Observations of the top view and of the cross sections were made.

For the observation of the top the samples have been simply mounted on the supports with the conductive adhesive, without embedding or polishing procedures. For the cross sections first the samples have been cut using a Struers Accutom-50® microcutter. Then the samples have been embedded in the conductive resin, mirror polished and mounted on the supports.

Also in this case EDS analysis were carried out in order to obtain information on the chemical composition of the oxide layer developed during the pin on disk test.

4 Results

This section presents the results of the experiments. In section 4.1 there are the results of the microstructural characterization made with optical and SEM analysis. In section 4.2 there are the results of the thermal treatments presented as the evolution of hardness versus the time of the treatments. Finally the results of the wear tests will be exposed: in section 4.3 the friction coefficient obtained by the pin on disk test, in section 4.4 the volume loss calculated from the results of the profilometer's analysis and in section 4.5 will be presented the SEM micrography of the wear tracks.

4.1 Microstructure

4.1.1 Fiber's dimension and distribution

The goal of the first part of the analysis was to study the microstructure of the material to have some preliminary useful information such as the fraction of the reinforcement inside the composite material and to reveal the effects of the thermal treatments on the microstructure, such as grain growth and intermetallic phases. To this aim, observations with optical and ESEM microscopes were carried out.

The first parameter to be evaluated was the distribution of the carbon fibers inside the material. First the cross section have been observed.

The samples analyzed were 8-3, 8-4 and 8-5, in accordance with the description given in section 2 and in Fig. 3-5.

The fibers highlight the flux flow of the material during the friction stir processing [54] as reported in Fig. 4-1 to 4-5. At the bottom of the samples (the top in the figures 4-1 and 4-2), a zone without fibers is clearly visible (zone 1 in Fig. 4-1). This is due to the fact that the pin did not reach this zone and so there was no stirring of the material and mixing with the carbon reinforcement. It is also possible to notice that there are different orientations of the fibers and that there are well-defined zones with the same orientations, parallel (zone 3 in Fig. 4-1) and

perpendicular (zone 2 in Fig. 4-1) to the section observed. These observations are the same for both the samples.

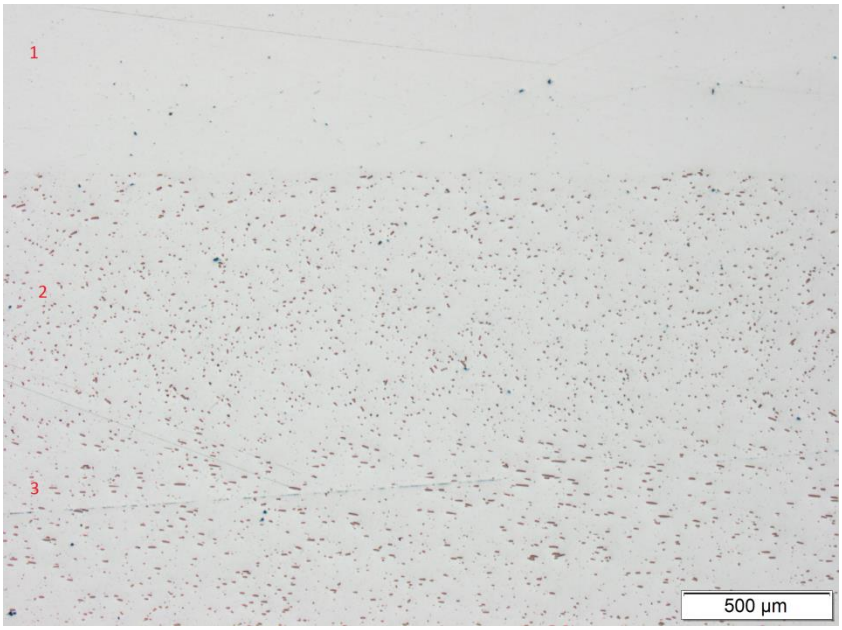

Figure 4-1 Cross section of the sample 8-4, 2.5X. It is possible to see the different orientations of the fibers and the zone without reinforcement.

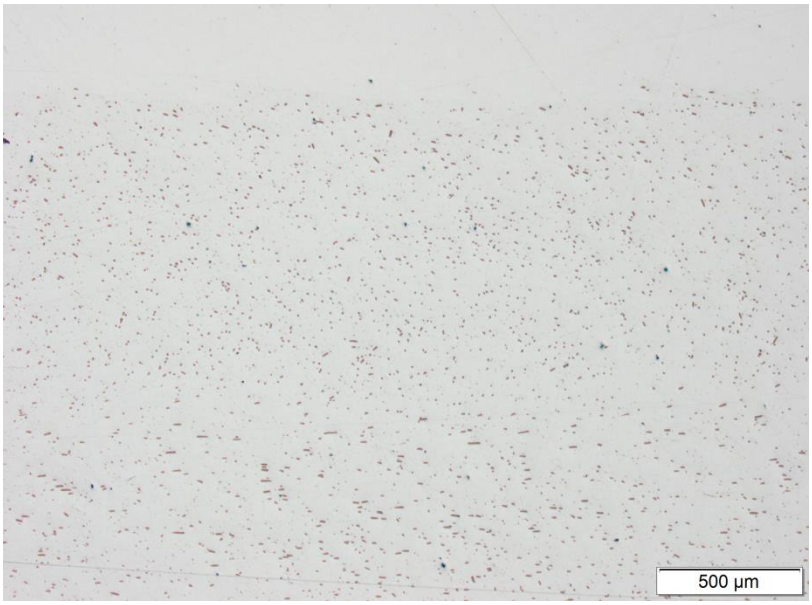

Figure 4-2 Cross section of the sample 8-5, 2.5X. It is possible to see that the fiber's distribution is similar to the one in Fig. 4-1.

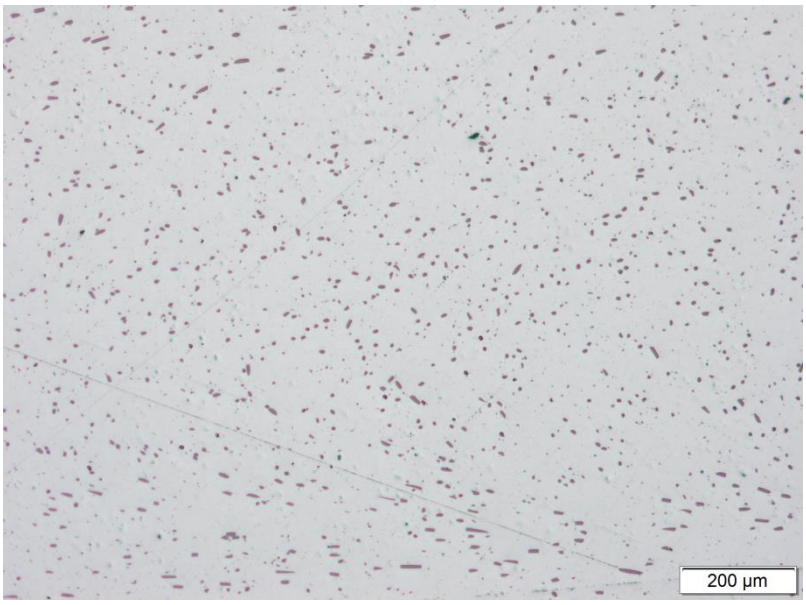

Figure 4-3 Cross section of the sample 8-3 taken at higher magnification, 5X. It is more clear the different orientation of the reinforce.

In the top section of the samples, it is possible to see different orientations of the fibers and zone without reinforcement. In this case the absence of fibers it is not due to the thickness of the sample and the dimension of the tool pin, but to the flow of the material during the process. This is visible in Fig. 4-4.

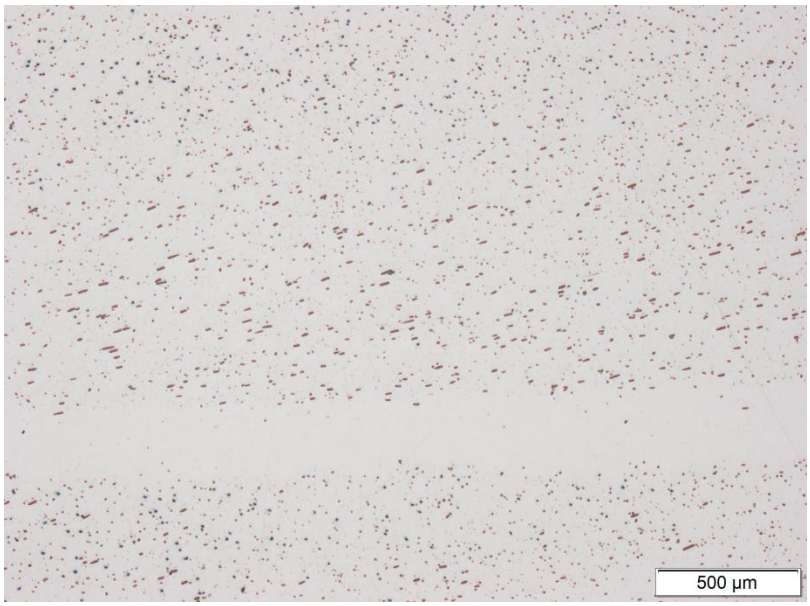

Figure 4-4 Top section of sample 8-4 at 2.5X. The zone without fibers and the different orientation of the fibers are clearly visible .

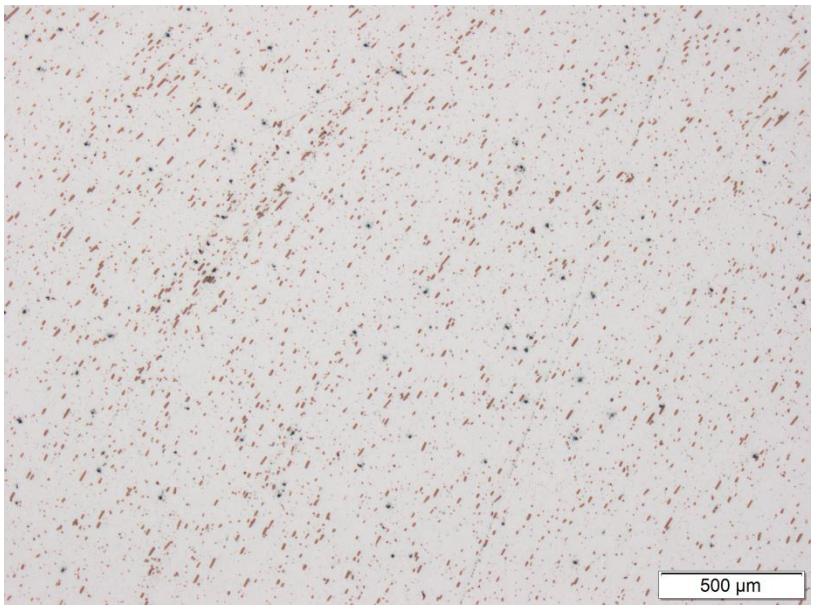

Figure 4-5 Top section of sample 8-3 at 2.5X of the second sample. The effect of the flow of the material in the fiber's distribution are clearly visible.

From the micrographs, the fiber's surface fraction has been evaluated using the software ImageJ® as described in paragraph 3.2.1. The pictures used for this analysis were taken from the top section of samples 8-3, 8-4 and 8-5. Ten pictures have been analyzed for each sample and the result is the average value.

	8-3	8-4	8-5	Total average
Average percentage	4.1915	3.7141	3.9318	3.9458

Table 4-1 Surface fraction of the reinforcement.

As we can see, the results are quite similar between the different samples.

To improve the quality of the results, the zones without fibers (see Fig. 4-4) were not considered.

From these micrographs, it is also possible to measure the fiber's dimension, but always with the uncertainty given by the orientations. We can see that the parallel fibers have maximum

length of 50µm, so we can assume that this is the maximum value. The method used for making of the composite do not allow to control the precise dimension of the reinforcement, due to the random breaking of the fibers. It is only possible to measure it afterwards [54].

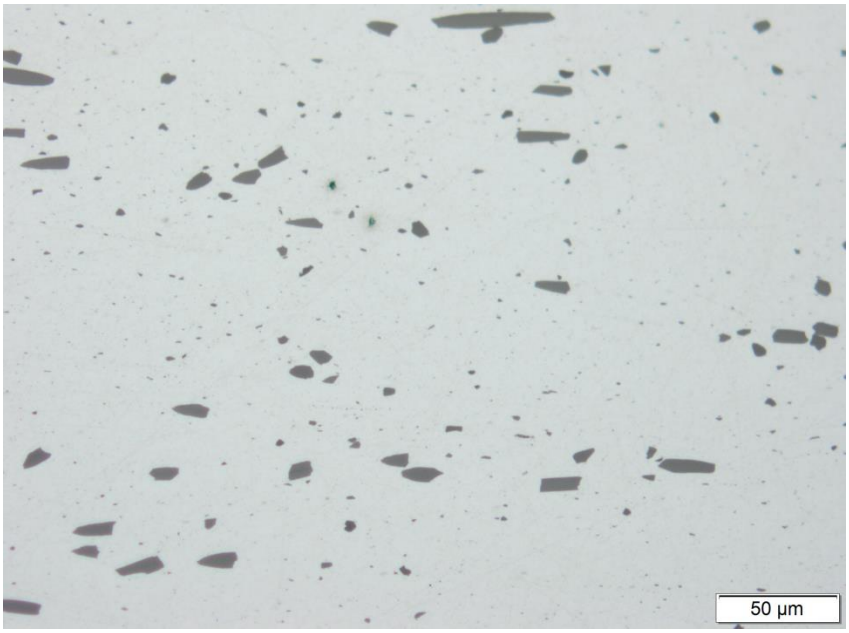

Figure 4-6 Sample 8-4, 20X. It is possible to notice that the fibers are not bigger than 50µm.

4.1.2 Grain size

The optical microscope was also used to measure the grain size inside the material. The samples studied for this purpose were 11-4, 11-5 and 12-2 without fibers, 8-3, 8-4 and 8-5 with fibers and 10-1, 9-6, 8-6 and 9-0 with fibers and after the solution treatment for 0, 1, 2 and 4 hours respectively.

For revealing the grain size it is necessary to etch the samples with the proper solution as mentioned in section 3.2.1. After etching the grain size has been revealed, but not in a way that allows us to measure it, as can be seen in Fig. 4-7. The grain boundaries were not highlighted sufficiently to use a software for automatic analysis (such as ImageJ® used for the fibers). The samples with the reinforcement exhibited a stronger reaction with the etchant that lead to a more

intense uniform corrosion. In Fig. 4-8 it is possible to notice some round holes made by the corrosion. For this reason, the results were not satisfactory, even when using a dilute solution. Higher magnifications were also used but without good results (See Fig. 4-9).

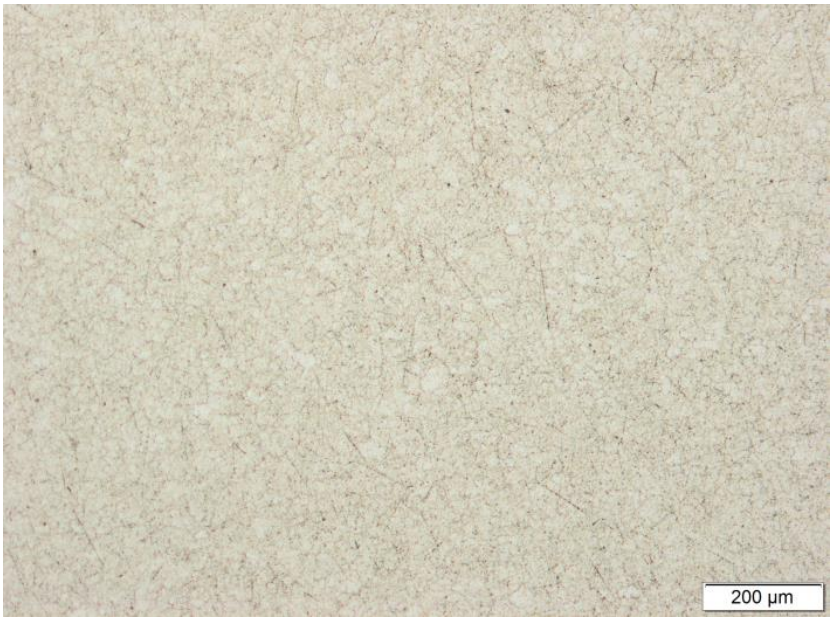

Figure 4-7 Sample 11-5 etched in 0.5% HF (conc.) in water for 3.5min, 5X. The grain boundaries are not sufficiently highlighted for a good estimation of the grain size.

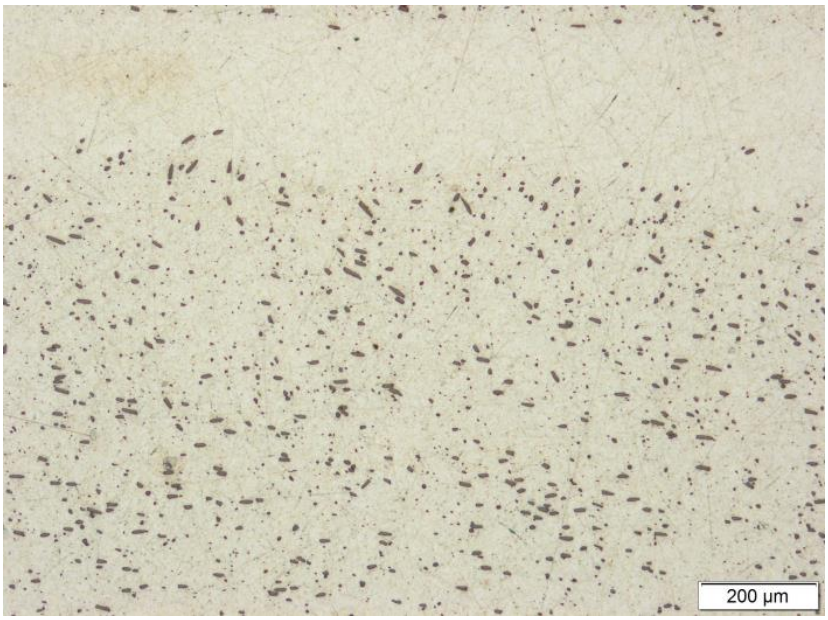

Figure 4-8 Sample 8-5 etched in 0.125% HF (conc.) for 1.5min, 5X. The presence of the fibers accelerates the reaction making grain size evaluation impossible.

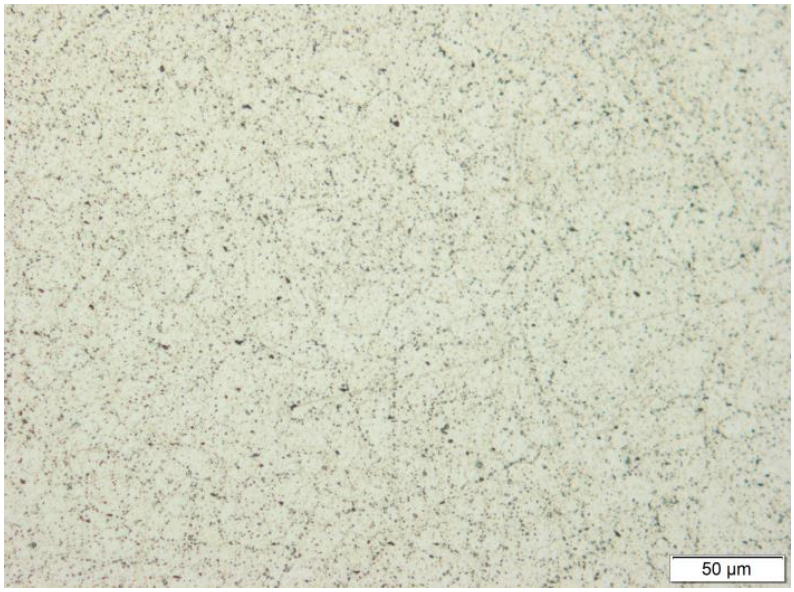

Figure 4-9 Sample 11-5 etched for 2.5 min, 20X. Here is more clear that the corrosion of the samples is not localized on the grain boundaries but tend to be more uniform all over the surface.

Better results were obtained with the samples that underwent the solution treatment, where the grain boundaries were clearly highlighted as can be seen in Fig. 4-10 and more clearly in Fig. 4-11 thanks to the higher magnification. The problem with these samples was that the number of grains highlighted was not sufficient to make a good estimation of the grain size. The grains have a dimension lower than 10µm with no signs of abnormal grain growth after the solution treatment.

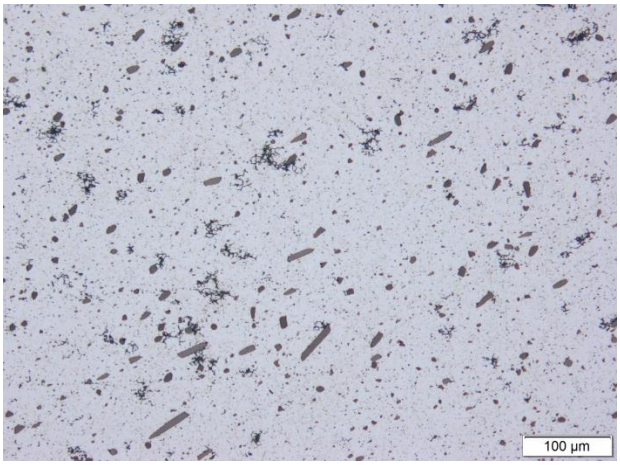

Figure 4-10 Sample 9-0 solution treated for 1 hour and etched in a 0.125 HF (conc.) aqueous solution for 3.5min, 10X. It is possible to see the areas where the grain boundaries are highlighted.

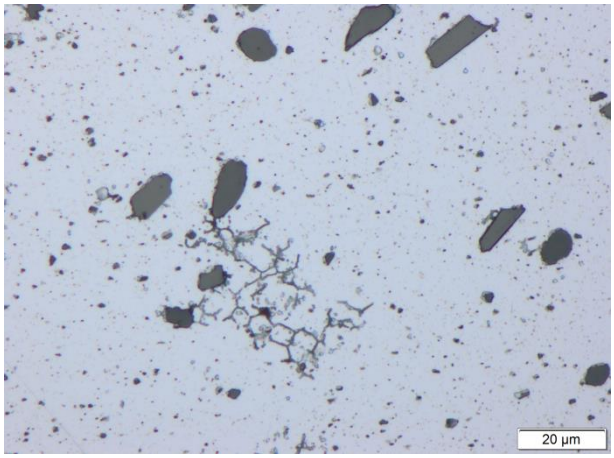

Figure 4-11 Sample 9-6 solution treated for 4 hours and etched in a 0.125 HF (conc.) aqueous solution for 3.5min, 50X. Zoom on an etched area.

In order to obtain more accurate results, the samples have been observed with the SEM. Microstructural modification during the thermal treatments have also been studied. For this purpose the samples has been observed before the treatments (samples 8-4 and 8-5) and after 1 and 48 hours of age hardening after the solubilization treatment. Thanks to the higher resolution of the instrument, it is possible to measure the grain size with a higher accuracy. A bigger number of grains have been highlighted. In this case, the measurements have been made manually using the software Stream Motion® given by Olympus. The average grain size measured was 3.7µm after the solution treatment, with a maximum value of 7µm and a

minimum of 1µm. Apparently no sign of abnormal grain growth were observed after the thermal treatment.

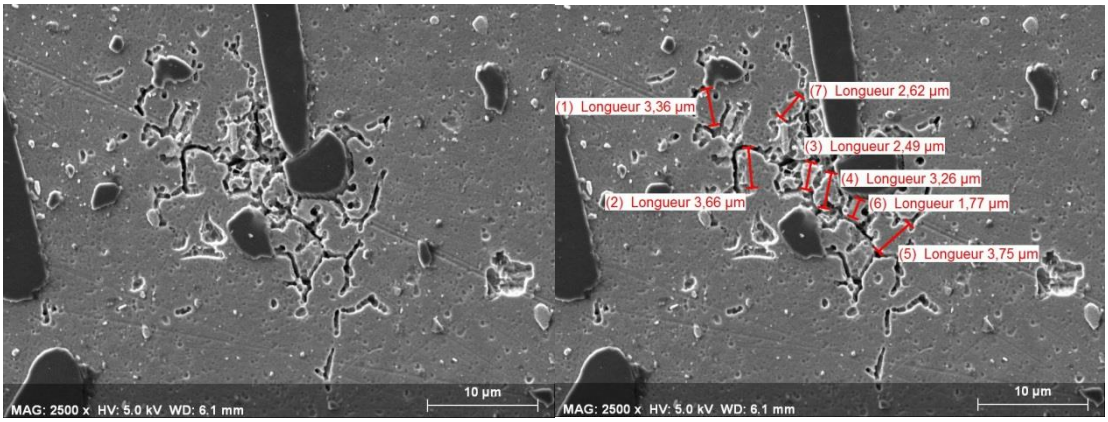

Figure 4-12 Sample 9-6 solution treated for 1 hour. On the left the original picture and on the right the measurement of the grain size.

Another important fact that was observed is the presence of small cracks starting from the tip of the carbon fibers (Fig. 4-13) and the presence of voids between the matrix and the reinforcement as in Fig. 4-14. These phenomena were observed only in the heat treated samples. These two phenomena will be important for the explanation of the wear mechanism of the heat treated samples (see chapter 5).

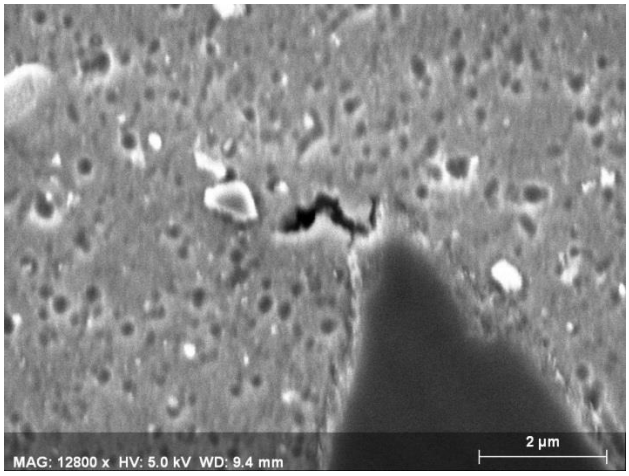

Figure 4-13 Crack on the tip of the carbon fiber.

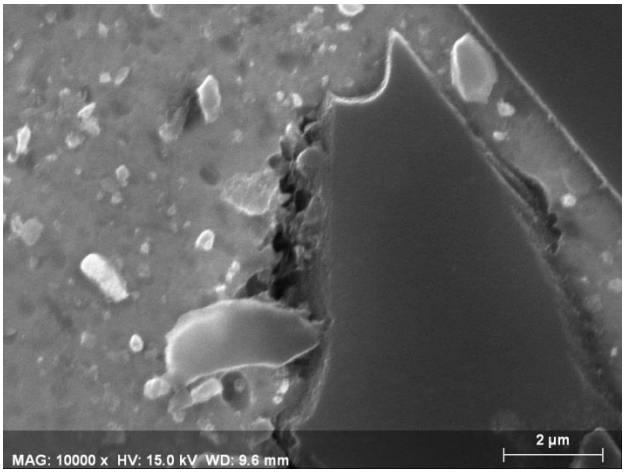

Figure 4-14 Void between the reinforce and the matrix.

4.1.3 Intermetallic compounds

SEM observations highlight the presence of intermetallic compounds in the heat treated samples, as predicted by literature. The precipitates were characterized by EDS to reveal their composition and the observation were made after 1 and 48 hours of age hardening in order to monitor their evolution. The dimensions of the particles were of the order of 1 µm. The EDS analysis presented in Fig. 4-15 suggests that the intermetallics were the α(AlFeMnSi) due to the presence of iron. Traces of magnesium were also found; the presence of carbon is due to the presence of the fibers. The composition was the same for all the samples studied.

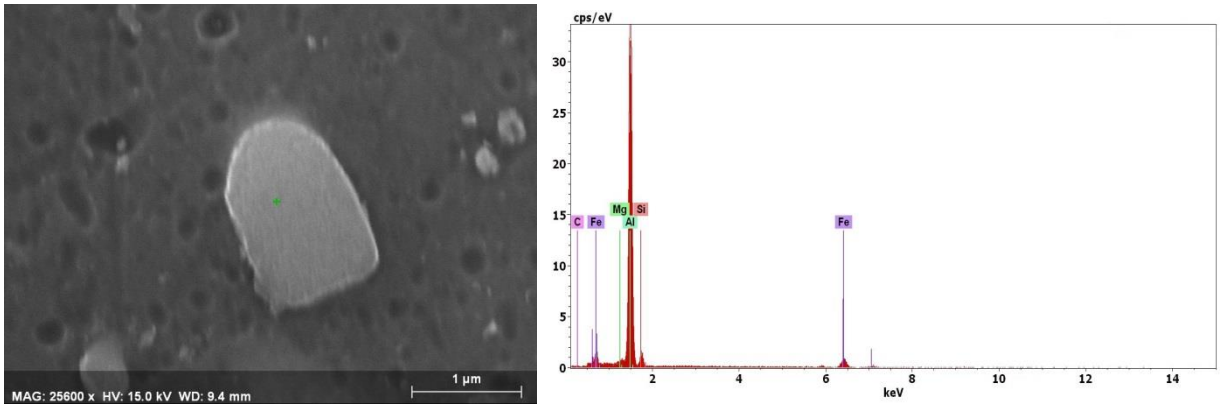

Figure 4-15 Intermetallic particle and corresponding EDS analysis.

Moreover, changes in the shape and in the number of the particles with the thermal treatments were observed. Comparing Fig. 4-16 (taken after 1 hour of age hardening) with Fig. 4-17 (taken after 48 hours of age hardening) it is possible to notice that the particle tend to have a more rounded shape and increase in number when increasing the age hardening. The same behavior was noticed when increasing the solubilization time, as can be seen comparing picture a) and b) on both Fig. 4-16 and 4-17. Moreover some precipitates with a very elongated shape were observed for low age hardening time as in Fig. 4-18. Particles with this morphology were not observed for the longer treatments.

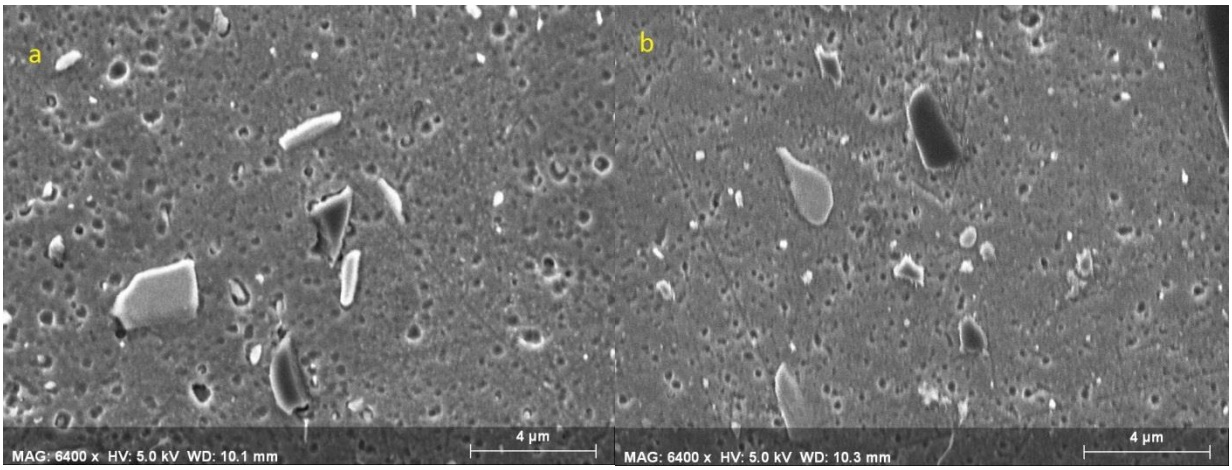

Figure 4-16 Evolution of the shape with the solubilization time: a) 0 hour and b) 4 hours for the same age hardening time.

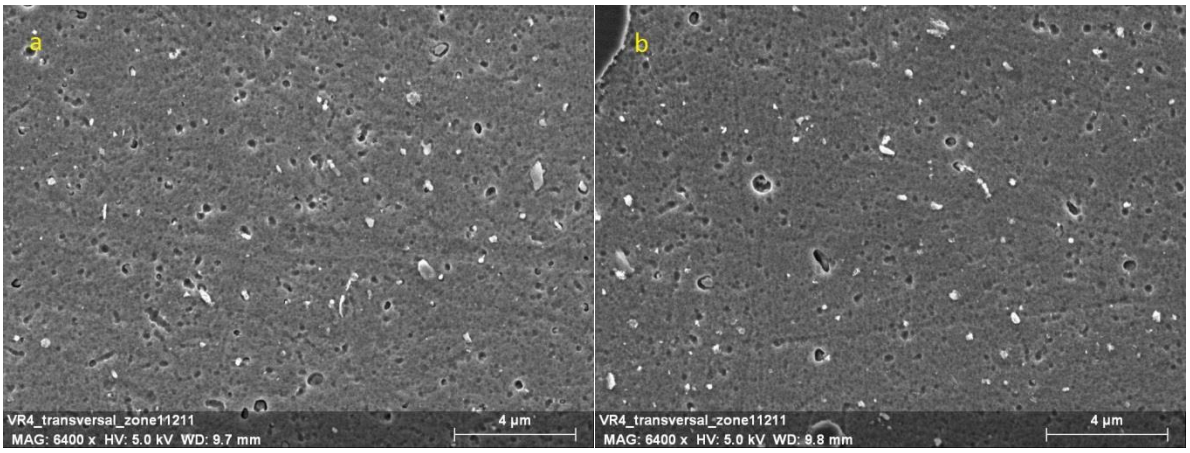

Figure 4-17 Intermetallic particles after 48 hours of age hardening. On the left the solubilization time was 0h and on the right 48 hours. It is possible to observe that the number of the precipitates increase in comparison to the same samples in Fig. 4-16.

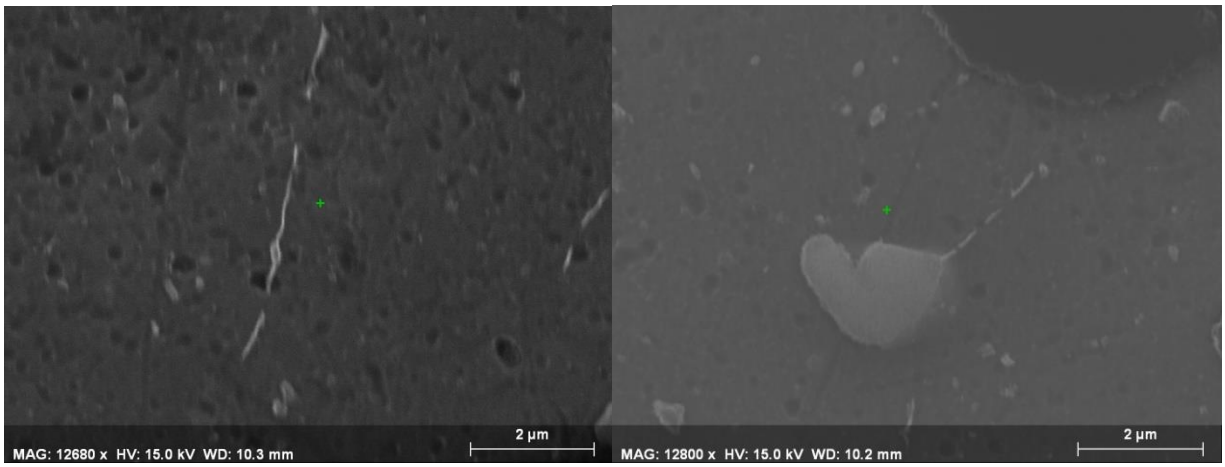

Figure 4-18 Thin precipitates observed for samples age hardened for 1 hour.

4.2 Hardness test

Hardness test have been carried out in order to monitor the effect of the thermal treatments on the material. Measurements were made only on the composite material after the solubilization treatment and during the age hardening to choose the best thermal treatment for the wear samples.

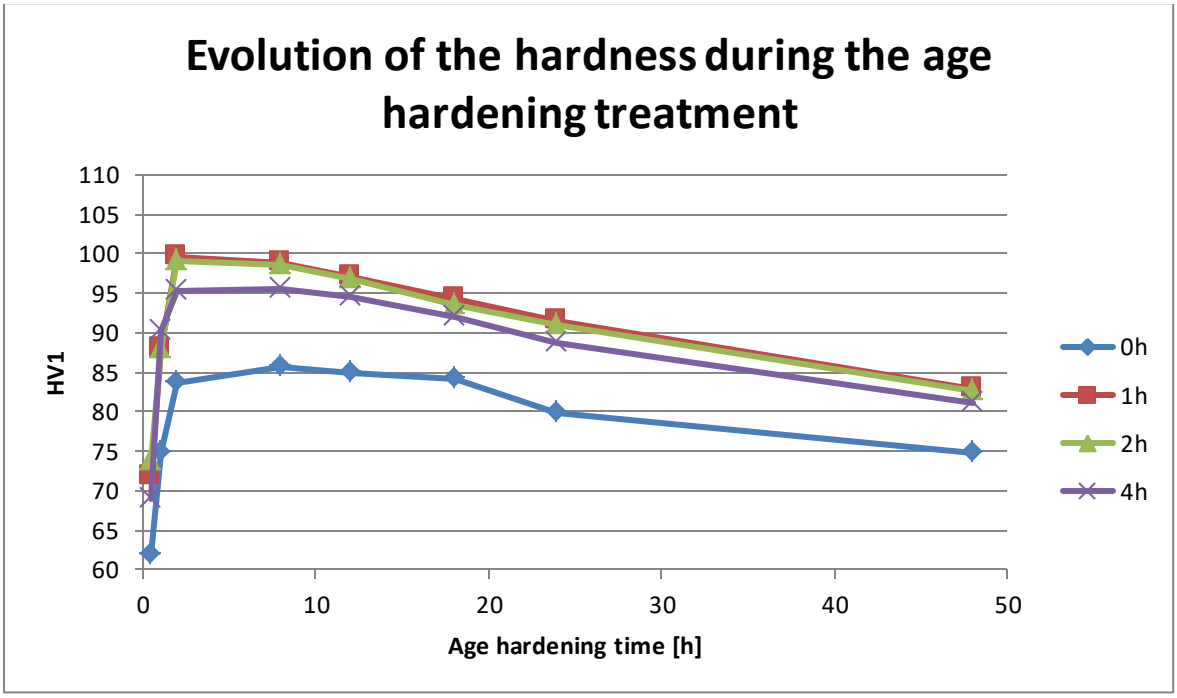

Figure 4-19 Evolution of the hardness with the ageing time. The four series correspond to the solubilization time.

Fig. 4-19 shows that the behavior of the four samples is quite similar, with a rapid increase of the hardness, followed by a maximum and a slow decrease with time. The effect of the solubilization time is also clear: the best results are reached for 1 or 2 hours. It is thus possible to notice that the thermal treatments have a great influence on the hardness of the material, with a great increase with the age hardening time. According to these results and to similar one found in literature [10,44,58,93], a solubilization treatment at 540°C for one hour followed by age hardening at 180°C for 10 hours has been chosen for the wear specimens. Between the two steps of the treatment, the samples were naturally age hardened for a week in order to have the precipitation of the GP zones that act as precursor for the precipitation of the β'' phase during the artificial age hardening.

4.3 Pin on Disk

A pin on disk tribometer was used to measure the friction coefficient, defined as the ratio between the normal load (set by the operator) and the transverse force measured by the apparatus. The instrument gives also the real time depth of the track, but we preferred to use as parameter the volume loss calculated from the profilometer's data.

First of all, the production of a black powder was observed during the testing of the composite samples. This means that the fibers were removed from the material.

Observing the plot of the friction coefficient presented in Fig. 4-20 and 4-21, it is possible to notice some common features between the samples. The most important fact is that in all the samples friction coefficient first decreases at the beginning of the test, and in a second stage its value tends to stabilize.

Looking at the plot of the friction coefficient of the sample 14-3 presented in Fig. 4-20 we can notice that, especially at the beginning, the value of the friction coefficient is not stable and some peaks are visible. In particular there are some values that reaches 0.4 and almost 1. This errors are clearly induced by the instrument.

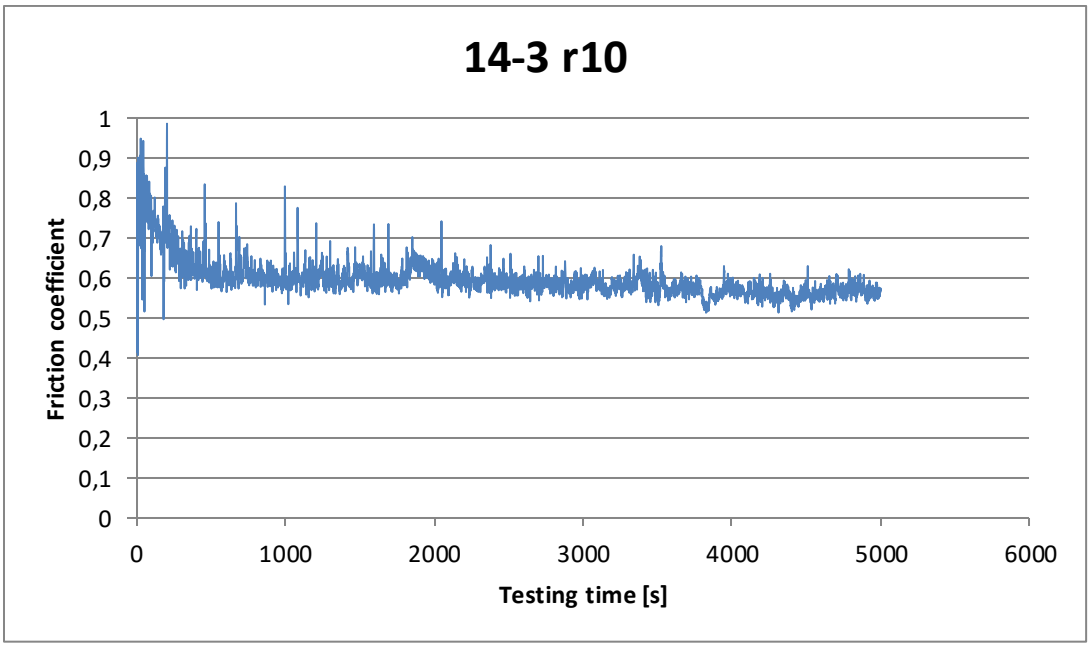

Figure 4-20 Plot of the friction coefficient for the reference material.

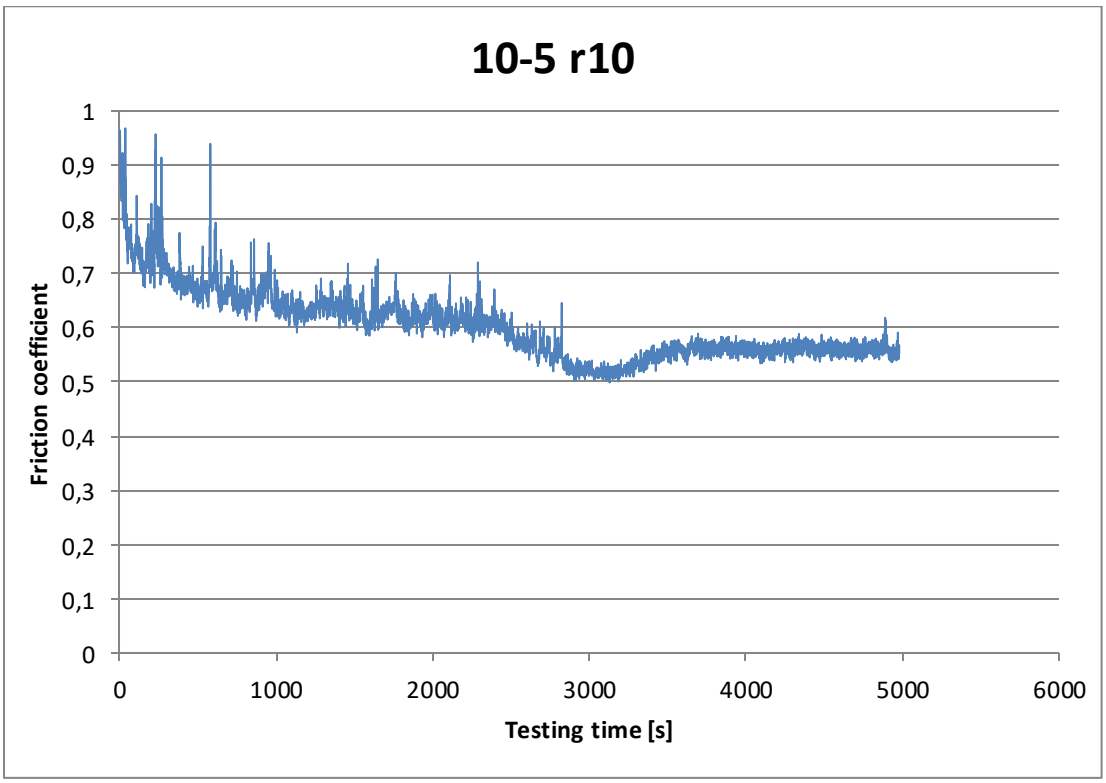

Figure 4-21 Plot of the friction coefficient for the MMC.

In the composite, a decrease of the friction coefficient for times between 2000 and 3500s (corresponding to 250 and 300m) was observed, always followed by a small increase of the

value. In some samples, the value then returns to almost the same level (see Fig. 4-22), but in others the value remains lower than before (like in Fig. 4-21).

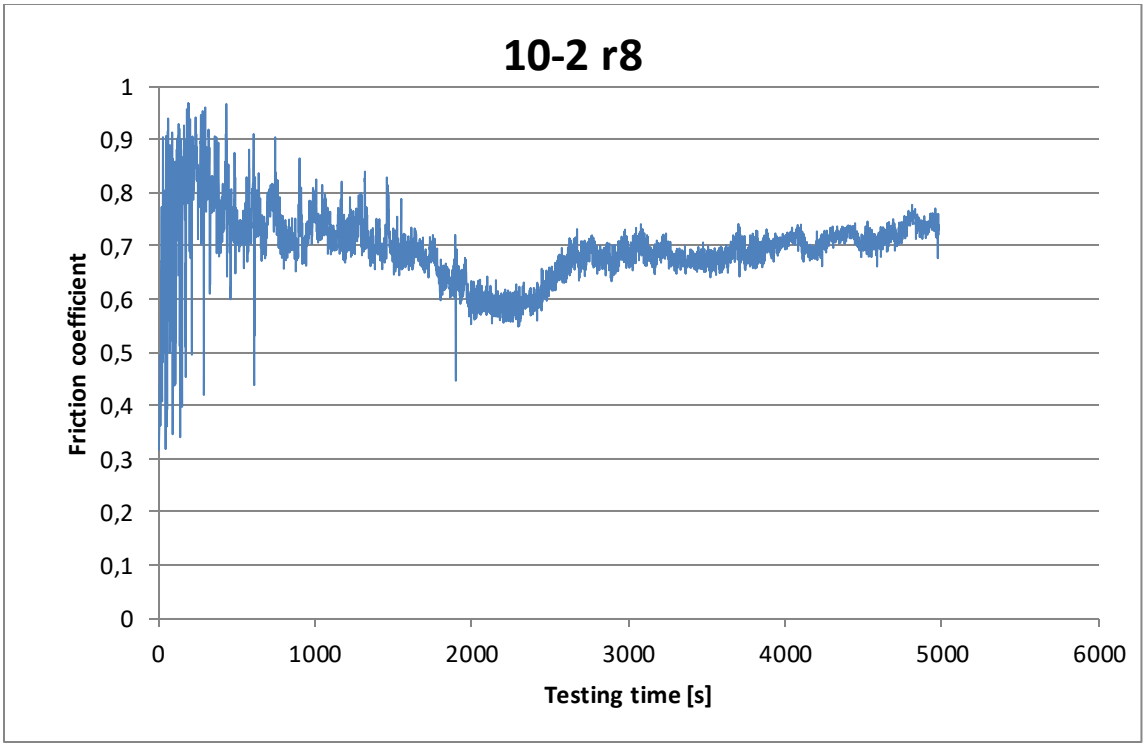

Figure 4-22 Plot of the friction coefficient for sample 10-2. Here, after the drop, the friction coefficient returns to the same value as before.

For a better understanding of the results, a plot with the average friction coefficient for each sample is presented (Fig. 4.23) The r8 bars (in blue) correspond to the 8mm tracks, made with 1N of normal load, while the r10 (in red) are the 10mm tracks made with the 3N load. As can be seen the general behavior is that the increase in the normal load causes a decrease of the friction coefficient. The decrease is not constant between the different samples, even if the samples have the same characteristics (in terms of reinforcement and thermal treatment). So, for example, the decrease in sample 12-3 is different compared to the decrease in sample 12-5, although the two samples have the same characteristics (they are both unreinforced, solution treated and age hardened). The only anomaly that we observe is in sample 14-2, where the friction coefficient is slightly higher for the 10mm track.

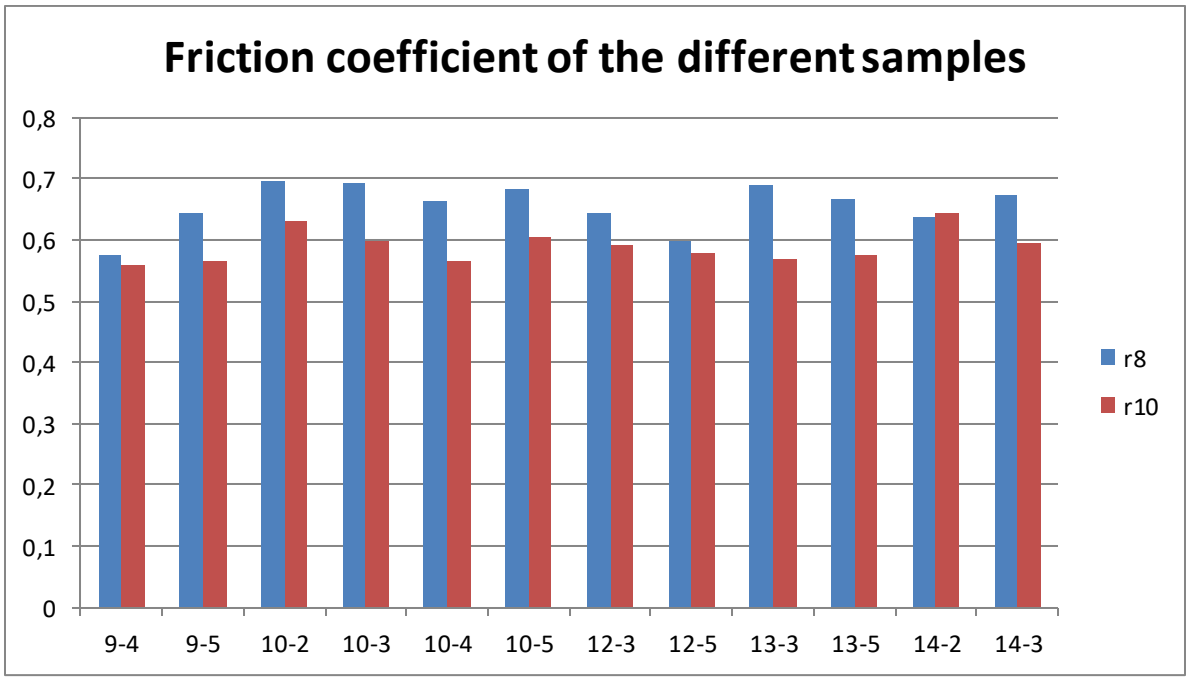

Figure 4-23 Plot of the average friction coefficient for each sample.

As shown in figure 4-23, two samples were tested for each condition. In figure 4-24, the average value for the two samples is presented. Figure 4-24 confirms that the friction coefficient decreases with increasing the normal load.

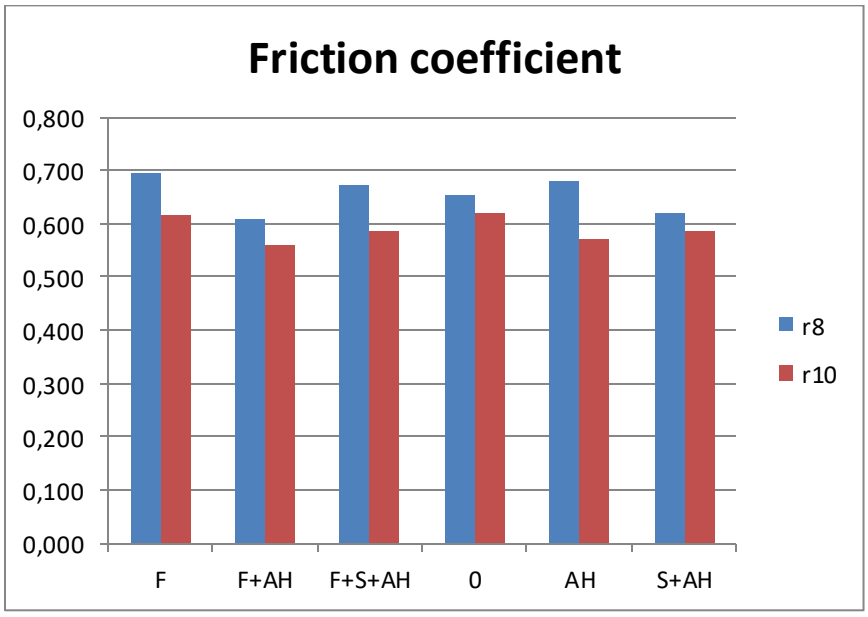

Figure 4-24 Plot of the average friction coefficient for the different condition of the samples.

It is difficult to make connection between the samples' condition and the value of the friction coefficient. We can see that the composite material with the full thermal treatment has not the lowest value. The results of the 8mm tracks seem to be more independent form the samples' condition, and the lower value is reached by the composite that is only age hardened. They vary from 0.610 to 0.695. Comparing the 3N track (r10 series), on the other hand, the differences between the various samples are less evident. Also in this case the age hardened material (without solubilization) has the lowest value of the friction coefficient. It is also possible to notice that the presence of the reinforcement does not influence the results (the values are almost the same). The results vary between 0.562 and 0.62. In both tracks the material with no thermal treatment has the worst properties.

Sample's configuration	r8	r10
F	0.695	0.614
F+AH	0.610	0.562
F+S+AH	0.673	0.585
0	0.654	0.620
AH	0.678	0.572
S+AH	0.621	0.585

Table 4-2 Numerical value for the friction coefficient.

4.4 Profilometer

The wear tracks were analyzed with a Profilometer, and the volume loss was calculated from these data. In the majority of the samples, the outer track (made with the highest load of 3N) is deeper in comparison to the inner one. The black parts are zone that were not detected by the instrument.

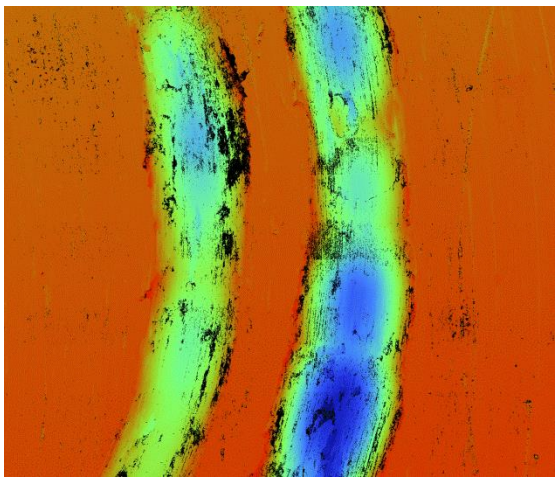

Figure 4-25 Sample 9-4. The colors vary from blue for the deepest zones to red. The 8mm track is the one on the left, while the other is the 10mm.

In Fig. 4-25, localized zones that are less deep in comparison to the rest of the track can be observed. From SEM observations, these zones were found to be clusters of material that accumulated during the test. If the cluster is small, it will not influence too much the result of the calculation of the volume loss.

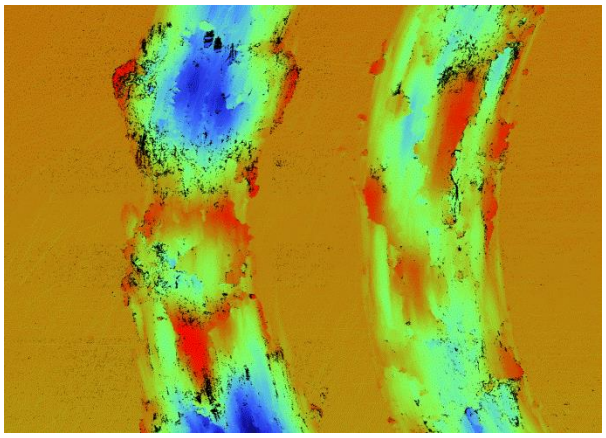

Figure 4-26 Sample 12-3. In this picture is possible to see more clearly the cluster in both tracks.

Another phenomena related to the wear of the sample is the accumulation of materials on the edges of the track, as shown in Fig. 4-27.

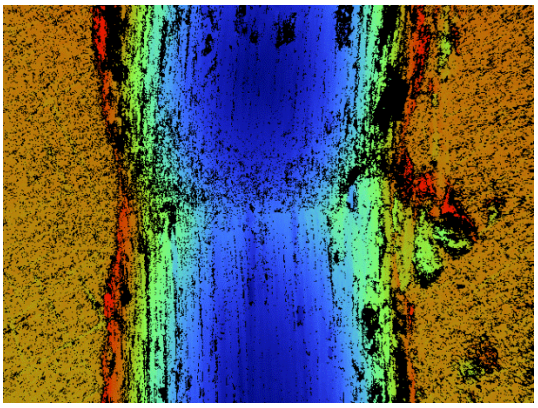

Figure 4-27 Sample 10-4, 10mm track. It is possible to notice the accumulation of material on the edge of the track.

The results of the elaboration of the data are presented in the following graph.

Fig. 4-28 presents the average values of the four segments measured in order to reduce the influence of these clusters on the results (see section 3.2.5). With the lower load (r8 bars) the difference between the samples is less important in comparison to the higher load. Also in this case the composite with the full thermal treatment does not show the best properties. We can see from the histogram that for the lowest load (1N, blue bars) the composite only age hardened has the lowest volume lost and for the highest normal load (3N, red bars) the aluminum alloy without reinforcement exhibits the lowest volume loss. (See Table 3-4 in section 3.1.3 for the numeration of the samples and their properties).

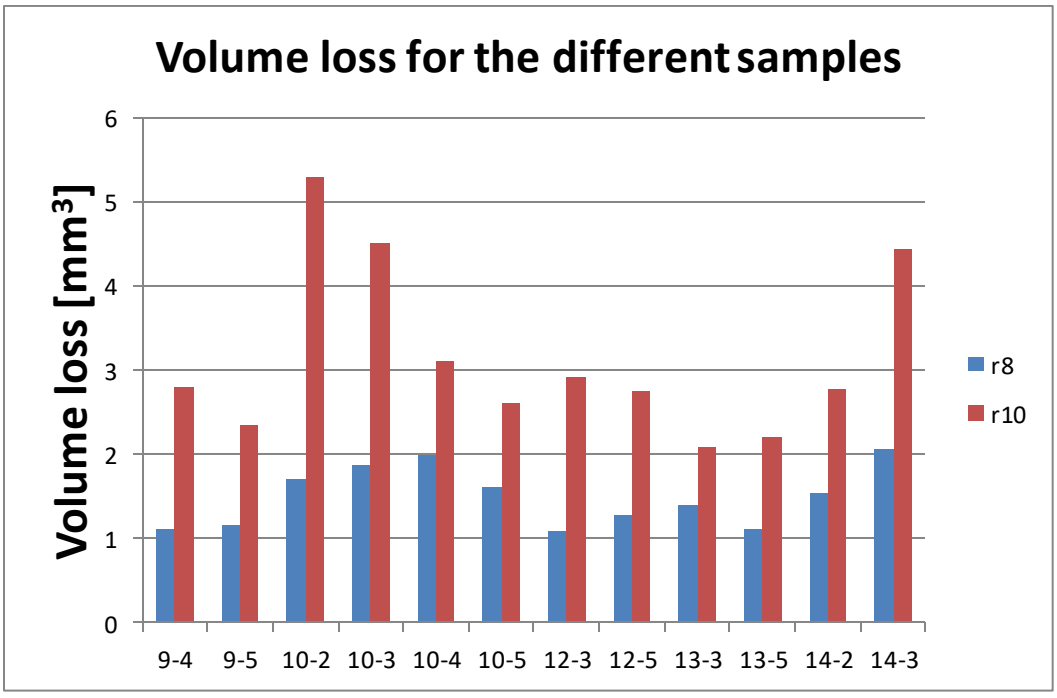

Figure 4-28 Volume loss for each sample.

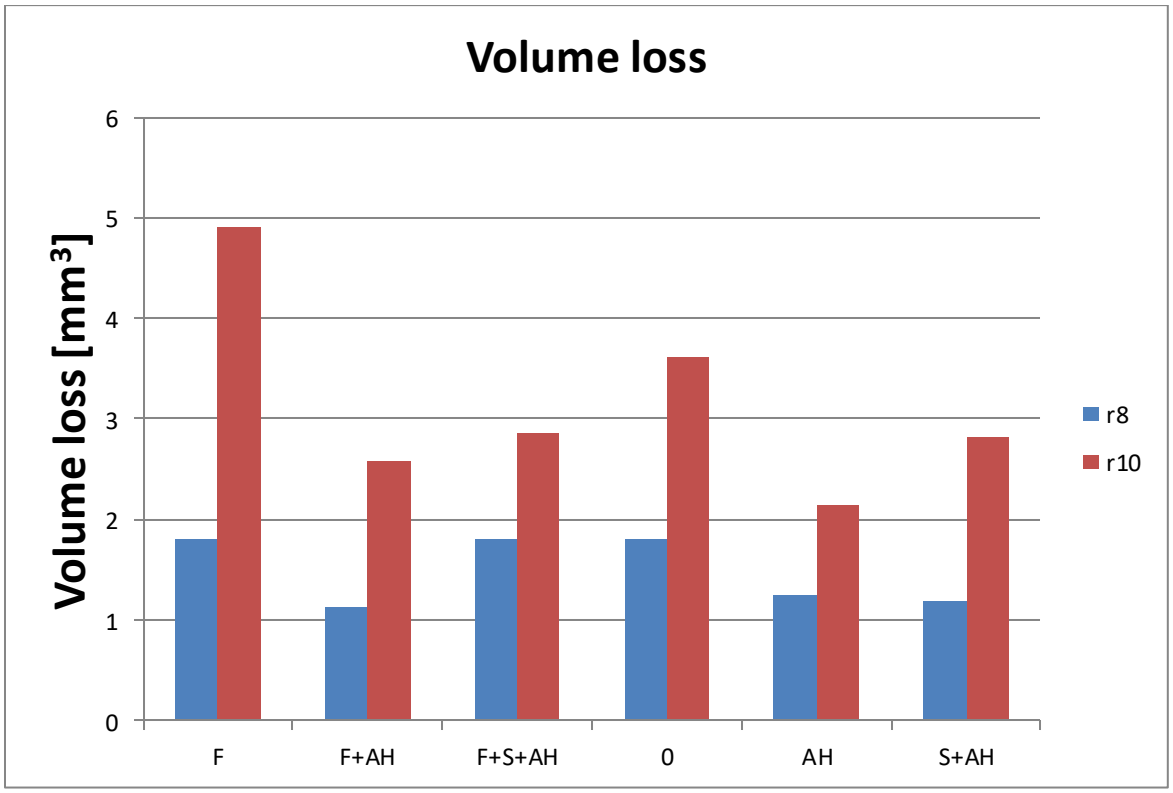

Figure 4-29 Volume loss for each sample's configuration.

4.5 ESEM analysis of the wear tracks

To understand better the wear mechanism, the tracks were observed with the ESEM combined with EDS. Both top and cross sections were studied. The main feature for all the samples is the development of an oxide layer over the tracks, as revealed by the EDS analysis in Fig. 4-30. The oxide layer is not uniform, but it is broken in some zones, revealing the aluminum alloy underneath.

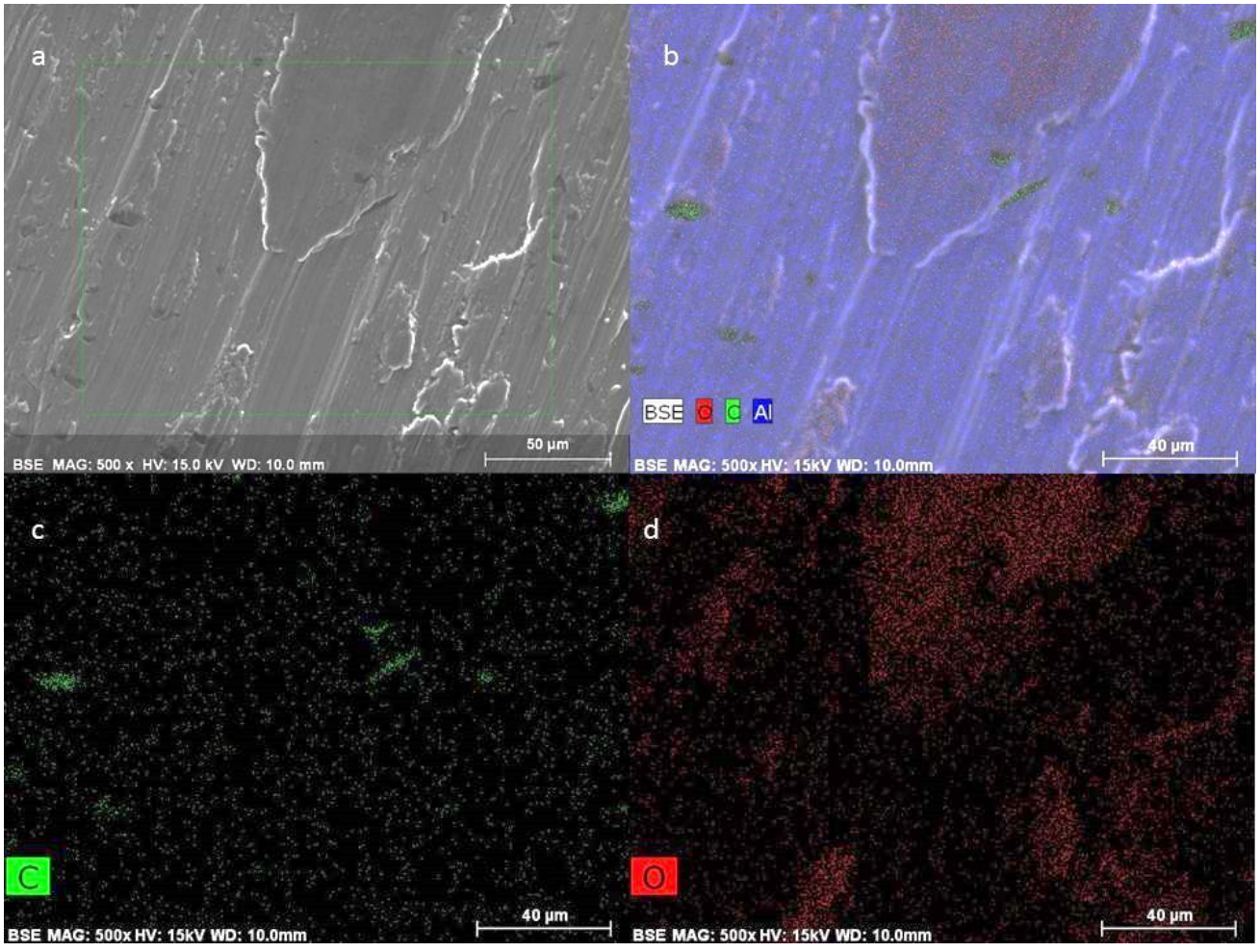

Figure 4-30 a) ESEM picture of sample 9-5, track 8mm. b) EDS mapping of the highlighted area for O, C and Al. c) Mapping only for C. d) Mapping only for O.

An EDS mapping was taken in a zone of the sample far from the tracks, in order to check if the presence of the oxide layer was really due to the wear mechanism or if this oxide was already present prior to the pin-on-disk test. SEM moreover allows to observe the oxide cluster highlighted by the profilometer's analysis (see figure 4-32).

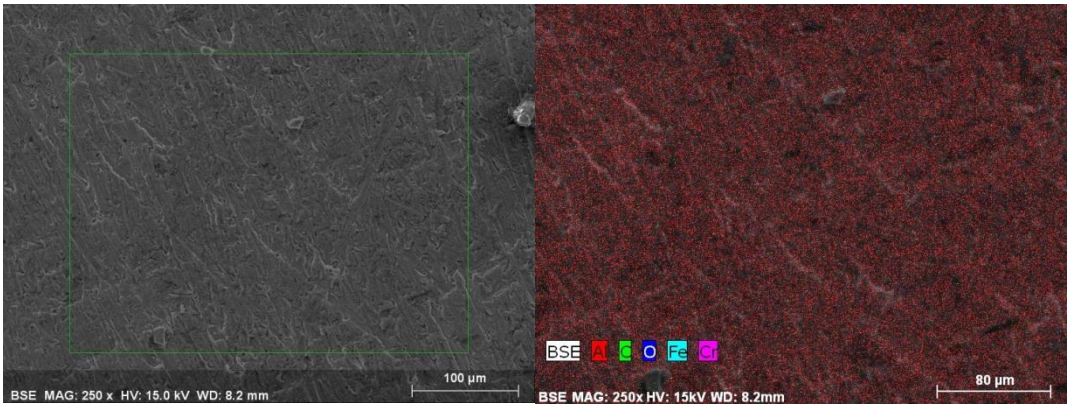

Figure 4-31 EDS mapping made on the center of sample 10-4. No oxides are revealed.

.

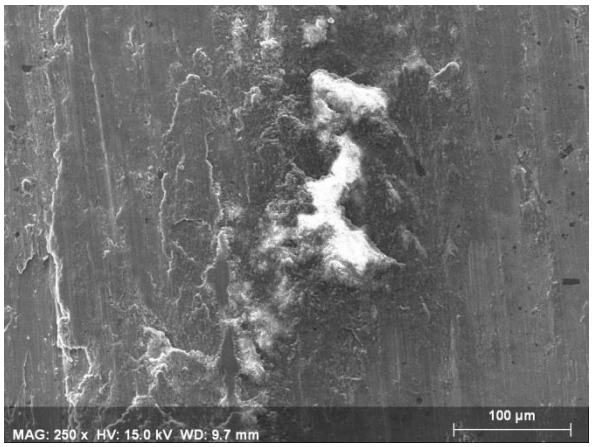

Figure 4-32 A cluster found in sample 9-4, 8mm track. The EDS analysis revealed that it is made of oxide.

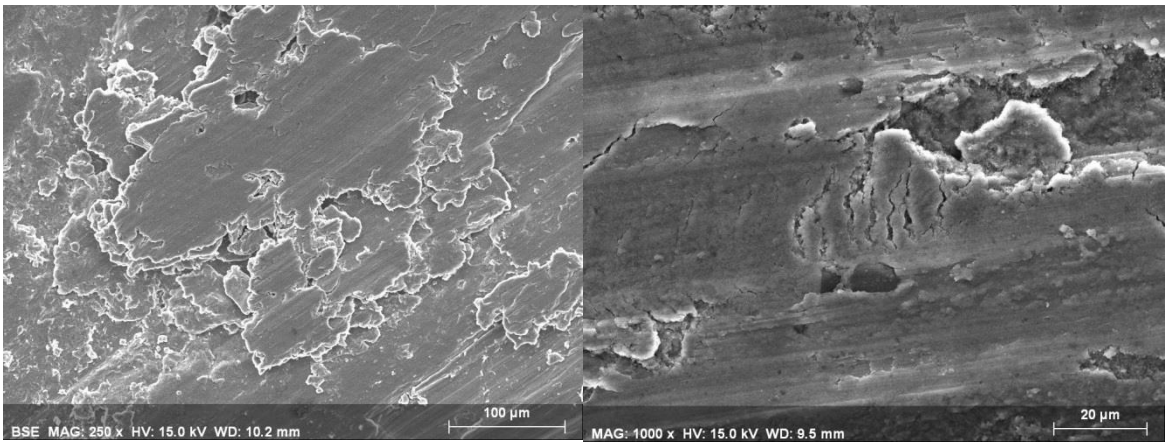

Figure 4-33 Broken oxide layer. On the left sample 12-3 10mm track. On the right sample 10-3 10mm track.

The presence of the oxide was observed in all the samples and no particular differences were noticed. No differences were noticed also comparing the two tracks made for each sample, revealing that the different loads have no influence on the morphology of the tracks. The morphology observed in some samples under the oxide layer suggest the presence of debris layer. This is commonly found in aluminum alloy.

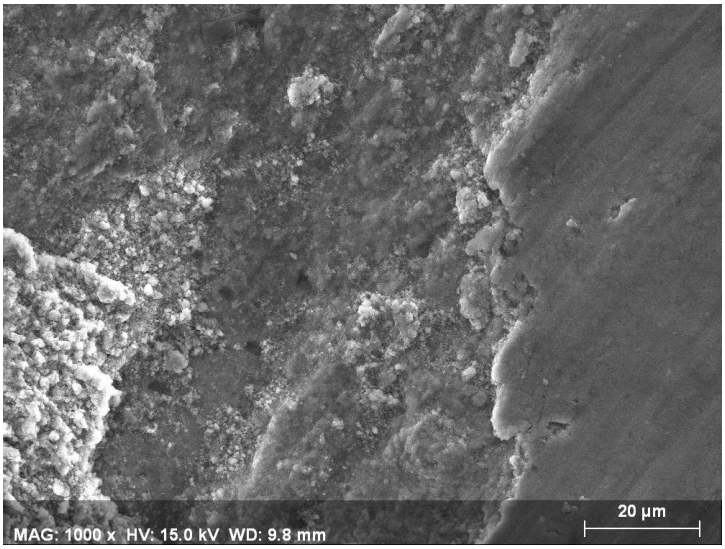

Figure 4-34 Debris material observed in sample 9-4, 8mm track.

The most remarkable difference was noticed in the MMC samples that were fully heat treated (solubilization plus age hardening). Only on these samples (10-4 and 10-5), there were holes left by the fibers extracted during the pin on disk test as can be seen from the SEM images in Fig. 4-35. No signs of fibers extractions were noticed in samples that were not solution treated.

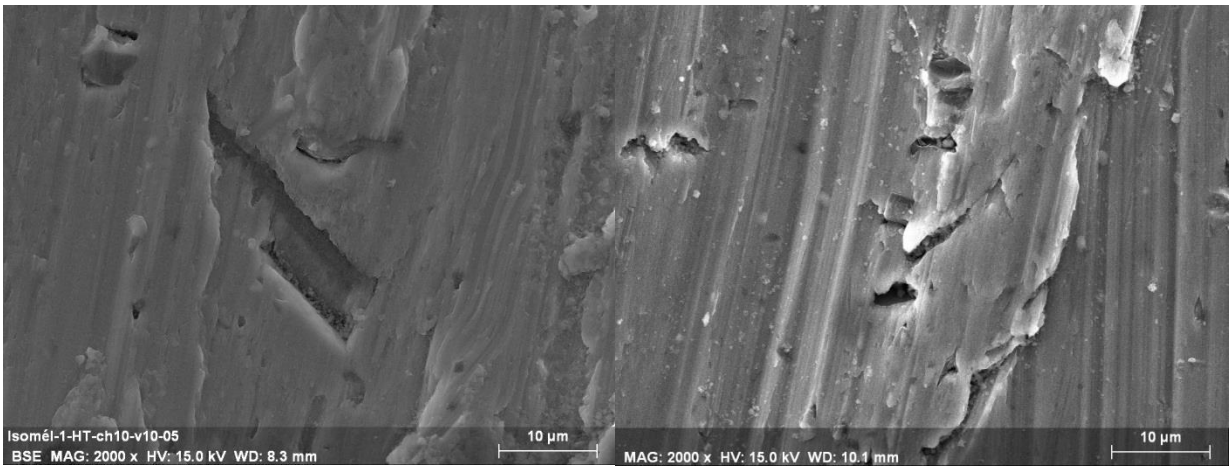

Figure 4-35 Holes left by the removed fibers. On the left sample 10-4 8mm and on the right sample 10-5 8mm.

For a better characterization of the oxide, cross sections of the samples were also observed with ESEM. From the top view, can be noticed that the oxide layer covers an important surface over the tracks. When the cross sections has been studied the oxide layer has been really hard to reveal. This is probably due to the samples preparation. When cutting the sample, the oxide layer may have been broken due to its inherent fragility. Alternatively, it may have been covered up by the resin during embedding. However, observations of cross section showed the accumulation of materials on the edge of the tracks (figure 4-36), and the layer formed by the compacted debris (figure 4-37 and 4-38).

.

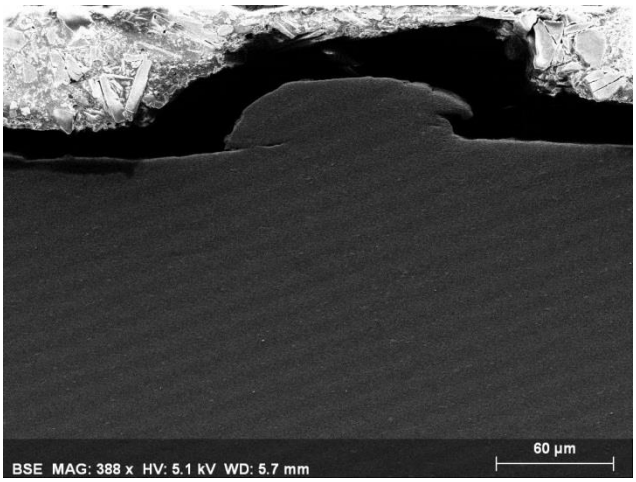

Figure 4-36 Sample 13-5, 8mm track. It is possible to notice the material on the edge of the track.

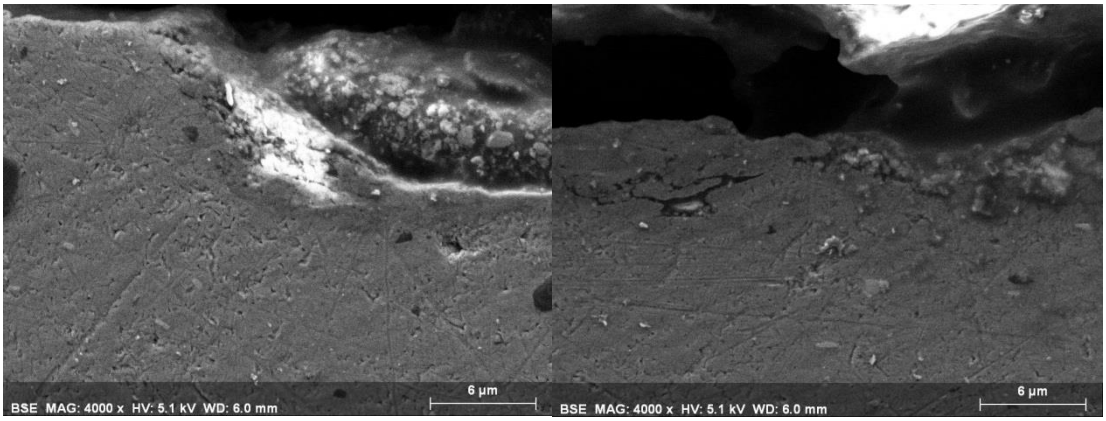

Figure 4-37 Sample 10-3, 10mm track. In the right picture we can see some cracks at the junction between the debris layer and the aluminum matrix.

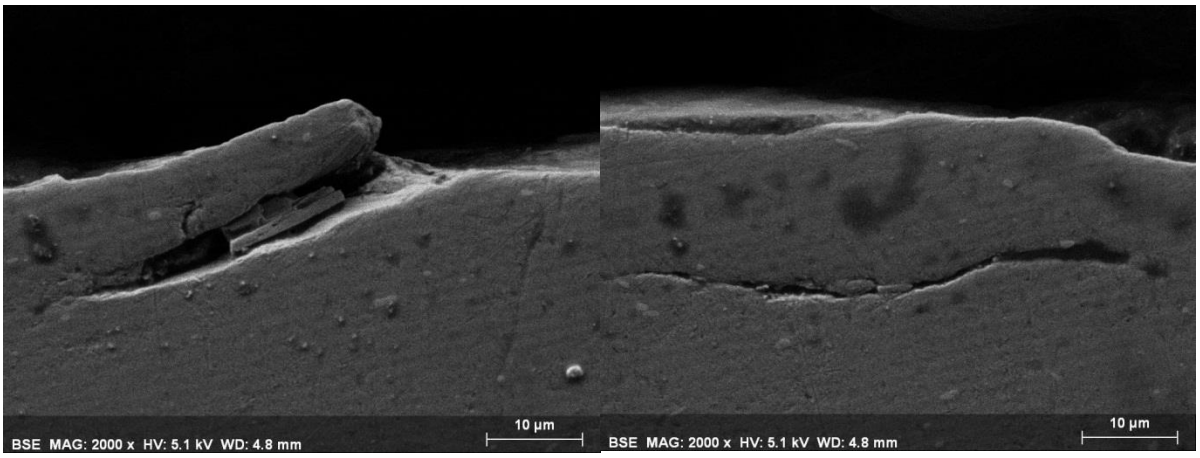

Figure 4-38 Sample 12-5, 10mm track. Other particulars of the debris layer

5 Discussion

In this chapter the results obtained and presented in the previous section will be discussed. In particular, the effect of the thermal treatments will be evaluated and then the results of the wear tests (pin on disk, profilometer and SEM images of the wear track) will be used for characterize the wear mechanism. In the last part the effect of the thermal treatments and of the reinforcement on the wear properties of the material will also be addressed.

5.1 Effects of thermal treatments.

The samples preparation made for the metallographic investigation, in particular the etching procedure, did not give optimal results as presented in section 4.1.2. In particular, as can be seen in the micrographs presented in Fig. from 4-7 to 4-11, the etching did not reveal a sufficient number of grain boundaries. For that reason there is not a complete understanding of the evolution of the microstructure of the material.

As can be seen from the plot in Fig. 4-19 thermal treatments gave good results, because there is a significant increase in the hardness of the material. The highest hardness was obtained after 1 hour of solution treatment at 540°C and between 8 and 10 hours of age hardening in accordance with other results found in literature [10]. In 6000 series aluminum alloy the most important hardening precipitates are the metastable β'' phase. With an age hardening time between 6 and 10 hours the β'' precipitates reach the optimal dimension and the maximum of the volume fraction [107] and, as a consequence, the material reach the highest hardness. For longer time the β'' precipitates evolve to the more stable β' and β phases that give a lower contribution to the hardness of the alloy. Moreover the SEM analysis show an increase also in the concentration of the α phase, as can be seen in Fig. 4-15, 4-16, 4-17 and 4-18. Longer times of both solubilization and age hardening cause also the coarsening of the precipitates. β'' is a metastable phase that act as a precursor for the following stable phases [119,120]. If there is an increase in the content of the stable phases, it means that the hardening β'' precipitates are dissolved, and this causes a decrease in the hardness of the material. This condition, with a relevant presence of stable precipitates due to longer age hardening treatments, is called over-ageing.

Two samples were also age hardened without solution treatment. This was made in order to investigate if during FSP there are some solubilization phenomena and how important they are. The precipitation mechanism for this alloy starts form a super saturated solid solution (SSSS), followed by the precipitation of the GP zones, that act as precursor for the β'' phase. During the friction stir processing of the same alloy (without the reinforcement) with similar parameters (rotational speed and transverse speed) the peak temperature reaches 400°C [10], that is not high enough to ensure the optimal solubilization of the precipitates to create the SSSS condition. Moreover this type of alloy shows natural ageing, so it is possible that precipitation phenomena occur during the time between the processing of the material and the moment of the test. Some solubilization process occurred, and this is confirmed by the increase in the hardness of the samples, but a post process solubilization treatment ensures better results.

On the solution treated samples it is possible to notice that there are cracks on the tip of the fibers (Fig. 4-16) or voids between the fibers and the matrix (Fig. 4-17). This is due to the difference in the thermal expansion coefficient of the two materials. During the heating at 540°C and the following water quenching the dilatation and the contraction of the two materials (carbon and aluminum) were different leading to stresses that cause the cracks. In the composite samples that were only age hardened the lower temperature used (180°C) and the slower cooling in air avoid the cracks' formation.

A problem related to friction stir welded aluminum alloy is abnormal grain growth observed by several studies [45-48] after thermal treatment at high temperature, such as the solubilization. On the material studied in this research apparently no traces of abnormal grain growth were observed after the exposure to high temperature. Difficulties during samples' preparation do not allow to be sure about the absence of abnormal grain growth, so an EBSD analysis (that allows to measure the grain size precisely) is suggested.

5.2 Wear behavior

5.2.1 Characterization of the wear mechanism

An important feature for the interpretation of the wear mechanism is the presence of an oxide layer (see in particular Fig. 4-30) on the surface of all the samples observed, as reported in section 4-5. Oxidation and oxidative wear as consequence, are common phenomena occurring in wear of aluminum alloy. In our case wear test were made at room temperature and with low load and sliding speed. As a consequence we can suppose that the frictional heat generated is not very high and the bulk temperature of the samples remain low. So the heat necessary to promote the oxidation in mainly the heat of deformation of the material [109]. Moreover in the asperities of the two surface in contact there will be a significant increase in temperature that can enhance the oxidation process [108].

As can be seen from Fig. 4-34 in section 4.5 the compact oxide layer is developed above the debris layer. So we can suppose that the oxide layer is developed from the metallic debris. The debris particle produced in the early stages are broken and reduced in size by the sliding action. For this reason fresh areas of clean metal are exposed for further oxidation [108].

The morphology of the debris layer is similar to the one found by Zhang and Alpas [63] on a 6061 aluminum alloy, typical for low load and sliding speed. As can be seen from Fig. 4-34 it is made of fine equiaxed particles. Another typical feature of the debris layer is the presence of cluster of material, highlighted both by the SEM (Fig. 4-32) and the profilometer analysis (Fig. 4-26). The mechanism of the formation of the debris layer can be the following: "*during sliding, wear debris particles are generated by the relative motion under load. Although some are lost, resulting in wear, others are retained within the tracks where they are comminuted by repeated plastic deformation and fracture while moving freely between the sliding surfaces. However, once they have been reduced to a sufficiently small size, they are agglomerated at certain locations, particularly in grooves, due to adhesion forces between solid surfaces arising from surface energy [110], and develop compact layers which eventually become load-bearing. During these processes, the fine particles are sintered together to some extent to form more solid*

layers; such sintering of fine particles can occur at temperatures only slightly above 20°C [110]." [108].

Moreover the parameters used for the wear test suggest that we worked in the mild wear regime. The results obtained with the further analysis confirmed this. The main microstructural difference between mild and severe regime is the presence of the debris layer. In particular in the mild regime we have the presence of this tribo-layer that is then damaged and removed in the severe wear. In the SEM analysis, the presence of the debris layer is obvious in all the samples (the most significant pictures are presented in section 4-5) and so we can confirm that the wear regime is the mild one.

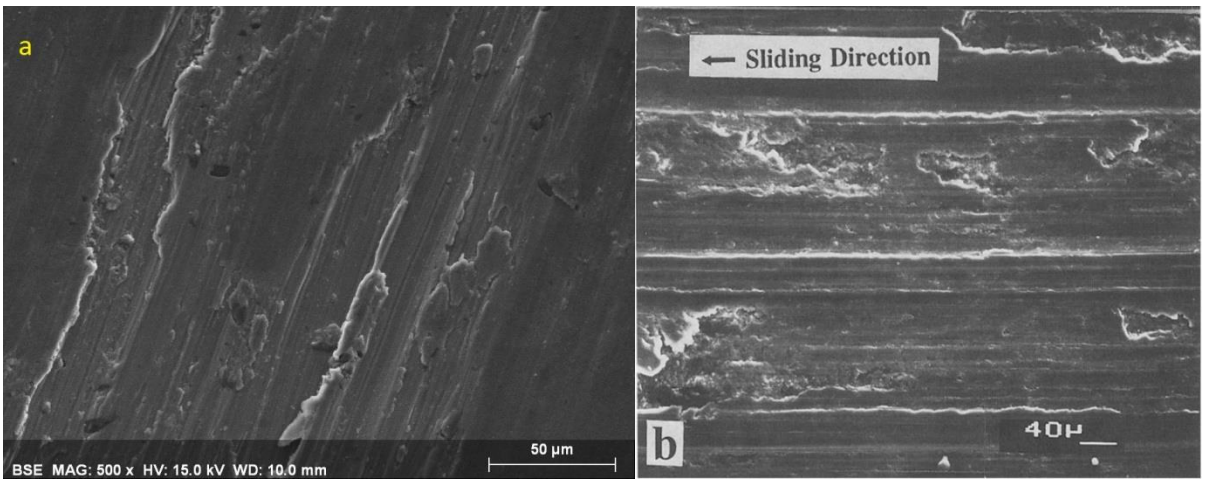

Figure 5-1 a) SEM image of the surface of the inner track (8mm) in sample 9-5. b) SEM image of a wear track made by Zhang and Alpas [63] in mid wear regime.

If we then compare Fig. 5-1 a) and b) it is possible to notice that they are very similar having another confirmation of the wear regime. From this deductions we can assume that the wear mechanism observed is an oxidative wear in the mild wear regime.

5.2.2 Effect of reinforcement and of heat treatment on wear properties

As reported in section 4.3 the behavior of the friction coefficient vs. testing time is similar for all the tracks. At the beginning there is a decrease of its value followed by a stabilization. This decrease is explainable with the formation of the debris and the oxide layer. It is well known that these layers protect the bulk material from wear due to their higher hardness. So at the beginning of the test the sliding surface were the steel ball (the pin) and the aluminum alloy (the disk). After some time the protective layer develops and so the two sliding surfaces become the steel ball and the hard layer (debris and oxide layer) decreasing the friction coefficient. After the layer is developed the value of the friction coefficient is more stable, as can be seen in Fig. 4-20, 4-21 and 4-22. The stabilization happened always between 500 and 1000s of testing.

As reported in section 4-3 a difference observed between the composite material and the unreinforced alloy is a small decrease of the friction coefficient followed by a small increase, observed only in the reinforced material. This suggest us that is due to the presence of the carbon fibers. An hypothesis made to justify that behavior is that at some moment during the test the fibers are free to move between the two sliding surfaces acting as solid lubricant [50]. But after some time they are removed from the tracks and so the lubricant effect cease. An interesting feature is that this phenomena always happened between 2000 and 3000s of testing, suggesting a relation between the length of the fiber and the depth of the tracks. No big differences are noticed comparing the average coefficients of the composite and of the unreinforced alloy. This is probably due to the fact that the decrease is low and only for a limited time, so this effect is hidden when the average value is considered. Both this two effects are presented in Fig. 5-4.

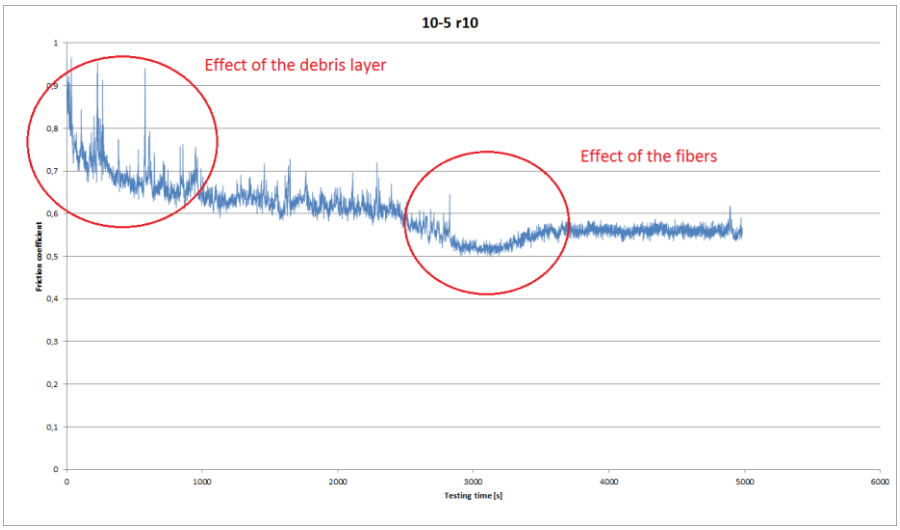

Figure 5-2 Evolution of the friction coefficient for the 10mm track of sample 10-5. The effects of the debris layer and of the fibers are highlighted.

As reported in sections 4.1.2 and 5.1 on the solution treated composite samples, voids between the matrix and the fibers and crack starting from the tip of the cracks were noticed (see Fig. 4-13 and 4.14). The absence of a connection between the reinforcement and the matrix lead to the extraction of the fibers during the wear test that has been observed and that are reported in Fig. 4-35, but, unfortunately, no differences were observed with the others composite samples.

Looking at the histograms made with the value for each kind of samples in Fig. 4-24 and 4-29 we can notice that the composite material in the T6 state (F+S+AH bars) does not exhibit the lower values. It is also possible to notice that for both parameters there is no apparent correlation between the sample's condition and the values obtained.

In all the samples it is possible to notice that increasing the value of the normal load from 1 to 3N (respectively blue and red bars) there is an increase in the volume loss and a decrease in the coefficient of friction as predicted by several previous works [50,77,90-98,100,101].

There are no clear differences between the composite material and the unreinforced material. This can be explained by the low value of both normal load and speed used in the test. Some studies [91,99] revealed that at lower normal load the behavior of the composite and of the unreinforced materials are similar. Moreover we observed the same wear mechanism in all the samples (debris layer and oxide). The oxide covers all the wear surface during the test. This hides the contribution of the matrix in the results and this nullify the effects of the thermal treatments

done on the samples. So we basically analyzed the wear properties of the oxide layer that, being the same in all samples, gives similar results.

As a conclusion no significant differences were noticed between the various sample's conditions, due to the oxidative wear mechanism and to the low loads and speed used during the wear tests, that were not sufficient to highlight the differences in the wear properties of the different samples.

6 Conclusions ad future prospects

The results obtained during the project and their interpretation will be summarized in this section. Moreover some suggestions will be provided to overcome the problems encountered.

The main objectives of this project were the optimization of a thermal treatment for a 6005Al-short carbon fibers metal-matrix composite in order to improve its wear resistance and the understanding of its wear mechanism.

The first part of this project was the microstructural characterization of the material with optical and SEM analysis. The experiments did not reveal signs of abnormal grain growth after the heat treatment. The effect of the etching solution used for the highlight of grain boundaries did not give good results (the material was corroded uniformly). For this reason an electron backscatter diffraction (EBSD) analysis is suggested in order to gain more precise data on grain size. Moreover it would be useful to investigate if the presence of the reinforcement lead to a refinement of the microstructure as previously reported by Mertens et al. in Mg-C composite produced with the same method [54].

The thermal treatment made on the material shows good results (see Fig. 4-19). A significant increase in the hardness of the material was reached after a solution treatment at 540°C for 1 hour followed by age hardening at 180°C for 10 hours, in agreement with the results found in literature [10].

The wear tests were made with a pin on disk tribometer at a sliding speed of 0.1m/s and with a normal load of 1 and 3N. SEM analysis of the wear tracks revealed the presence of a compact oxide layer above the debris layer. This suggests that the wear mechanism of the material is oxidative in the mild regime. No clear effect of the thermal treatments and of the carbon fibers on the wear properties was observed (see Fig. 4-24 and 4-29). This happened because the oxidative wear mechanism is not influenced by the ”bulk” properties of the material. Moreover the difference between the two loads tested is too small to highlight different behaviors. For this reason a wider range of both normal loads and sliding speeds should be investigated in order to study the properties of the material in different wear regime to have a complete characterization of the material. Moreover different wear mechanism can highlight the effects of the carbon fibers and of the thermal treatments. Riahi and Alpas [64] observed that one of the effect of the

reinforcement on wear properties is to delay the transition between the mild and severe wear regime, and it would be important to see if this happens also with the short carbon fibers. A small effect of the carbon fibers on the friction coefficient have been observed on the material, as reported in sections 4.3, 5.2.2 and in Fig. 5-2. It would be useful to make further analysis on this phenomenon. This can be done by stopping the wear test and doing some SEM observations to see if there are changes in the microstructure of the sample (especially of its surface) and to better understand the role of the reinforcement on the wear behavior.

One might also test the mechanical properties of the composite material and compare them with the properties of the FSP aluminum alloy (without reinforcement). Some studies [20] reported that graphite particles, used as reinforcement to improve wear resistance of an aluminum alloy, produce a decrease in the mechanical properties so it would be interesting to see what is the effect of short carbon fibers.

7 Bibliography

[1] W.M. Thomas, E.D. Nicholas, J.C. Needham, M.G. Murch, P. Templesmith, C.J. Dawes, G.B. Patent Application No. 9125978.8 (December 1991)

[2] C. Dawes, W. Thomas, TWI Bulletin 6, November/December 1995, p. 124

[3] R.S. Mishra, Z.Y. Ma, Materials Science and Engineering R 50 (2005) 1-78

[4] C.G. Rhodes, M.W. Mahoney, W.H. Bingel, R.A. Spurling, C.C. Bampton, Scripta Mater. 36 (1997) 69

[5] S. Benavides, Y. Li, L.E. Murr, D. Brown, J.C. McClure, Scripta Mater. 41 (1999) 809

[6] W.M. Thomas, E.D. Nicholas, S.D. Smith, in: S.K. Das, J.G. Kaufman, T.J. Lienert (Eds.), Aluminum 2001-Proceedings of the TMS 2001 Aluminum Automotive and Joining Sessions, TMS, 2001, p. 213

[7] W.M. Thomas, K.I. Johnson, C.S. Wiesner, Adv. Eng. Mater. 5 (2003) 485

[8] Peng Dong, Hongmei Li, Daqian Sun, Wenbiao Gong, Jie Liu, Materials and Design 45 (2013) 524-531

[9] A. Simar, Y. Bréchet, B. de Meester, A. Denquin, T. Pardoen, Mater. Sci. Eng. A 486 (2008) 85-95

[10] A. Simar, Ph.D. Thesis, Université Catholique de Louvain, Belgium

[11] G. Liu, L.E. Murr, C.S. Niou, J.C. McClure, F.R. Vega Scripta Mater. 37 (1997) 355

[12] K.V. Jata, S.L. Semiatin, Scripta Mater. 43 (2000) 743

[13] B. Heinz, B. Skrotzki, Metall. Mater. Trans. B 33 (6) (2002) 489

[14] L.E. Murr, Y. Li, R.D. Flores, E.A. Trillo, Mater. Res. Innovat. 2 (1998) 150

[15] Y. Li, L.E. Murr, J.C. McClure, Mater. Sci. Eng. A 271 (1991) 213

[16] Z.Y. Ma, R.S. Mishra, M.W. Mahoney, Acta Mater. 50 (2002) 4419

[17] M.W. Mahoney, C.G. Rhodes, J.G. Flintoff, R.A. Spurling, W.H. Bingel, Metall. Mater. Trans. A 29 (1998) 1955

[18] W. Tang, X. Guo, J.C. McClure, L.E. Murr, J. Mater. Process. Manufact. Sci. 7 (1998) 163

[19] Y.J. Kwon, N. Saito, I. Shigematsu, J. Mater. Trans. A 30 (1999) 2429

[20] A. Baradeswaran, A. Elaya Perumal Composites: Part B 56 (2014) 464-471

[21] L.E. Murr, G. Liu, J.C. McClure, J. Mater. Mater. Lett. 16 (1997) 1081

[22] G.S. Frankel, Z. Xia, Corrosion 55 (1999) 139

[23] Y.S. Sato, S.H.C. Park, H. Kokawa, Metall. Mater. Trans. A 32 (2001) 3023

[24] S.H. Kazi, L.E. Murr, in: K.V. Jata, M.W. Mahoney, R.S. Mishra, S.L. Semiantin, D.P. Filed (Eds.), Friction Stir Welding and Processing, TMS, Warrendale, PA, USA, 2001, p. 139

[25] H.G. Salem, A.P. Reynolds, J.S. Lyons, Scripta Mater. 46 (2002) 337

[26] R. Braun, L. Litynska-Dobrzynska, Mater. Sci. Forum 396-402 (2002) 1531

[27] A.F. Norman, I. Brough, P.B. Prangnell, Mater. Sci. Forum 331-337 (2000) 1713

[28] K.A.A. Hassan, A.F. Norman, P.B. Prangnell, Mater. Sci. Forum 396-402 (2002) 1549

[29] J.Q. Su, T.W. Nelson, R.S. Mishra, M.W. Manohey, Acta Mater. 51 (2003) 713

[30] Z.Y. Ma, R.S. Misra, M.W. Mahoney, R. Grimes, Mater. Sci. Eng. 351 (2003) 148

[31] I. Charit, R.S. Mishra, Mater. Sci. Eng. A 359 (2003) 2009

[32] I. Charit, R.S. Mishra, M.W. Mahoney, Scripta Mater. 47 (2002) 631

[33] I. Charit, Z.Y. Ma, R.S. Mishra, in: Z. Jin, A. Beaudoin, T.A. Bieler, B. Radhakrishnan (Eds.), Hot Deformation of Aluminum Alloys III, TMS, 2003, pp.331-342

[34] P.S. Pao, E. Lee, C.R. Feng, H.N. Jones, D.W. Moon, in: K.V. Jata, M.W. Mahoney, R.S. Mishra, S.L. Semiatin, T. Lienert (Eds.), Friction Stir Welding and Processing II, TMS, Warrandale, PA, USA, 2003, p. 113

[35] Y.J. Kwon, I. Shigematsu, N. Saito, Mater. Trans. 44 (2003) 1343

[36] Y.J. Kwon, I. Shigematsu, N. Saito, Scripta Mater. 49 (2003) 785

[37] K.V. Jata, K.K. Sankaran, J.J. Ruschau, Metall. Mater. Trans. A 31 (2000) 2181

[38] M. James, M. Mahoney, in: Proceedings of the First International Symposium on Friction Stir Welding, Thousand Oaks, CA, USA, June 14-16, 1999

[39] Z.Y. Ma, R.S. Mishra, M.W. Mahoney, in: K.V. Jata, M.W. Mahoney, R.S. Mishra, S.L. Semiatin, T. Lienert (Eds.) Friction Stir Welding and Processing II, TMS, 2003, p. 221-230

[40] J.Q. Su, T.W. Nelson, C.J. Sterling, J. Mater. Res. 18 (2003) 1757

[41] K. Matsuki, T. Iwaki, M. Tokizawa, Y. Murakami, Mater. Sci. Technol. 7 (1991) 513

[42] Y. Sato, M. Urata, H. Kokawa, Metall. Mater. Trans. A 33 (2002) 625

[43] Y.S. Sato, H. Kookawa, M. Enmoto, S. Jogan, Metall. Mater. Trans. A 30 (1999) 2429

[44] Grażyna Mrówka-Nowotnik, Jan Sieniawski, Journal of Materials Processing Technology 162-163 (2005) 367-372

[45] H.J. Liu, X.L. Feng, Materials and Design 47 (2013) 101-105

[46] S. Jana, R.S. Mishra, J.A. Baumann, G. Grant, Materials Science and Engineering A 528 (2010) 189-199

[47] I. Charit, R.S. Mishra, Scripta Materialia 58 (2008) 367-371

[48] Kh. A.A. Hassan, A.F. Norman, D.A. Price, P.B. Prangnell, Acta Materialia 51 (2003) 1923-1936

[49] H. Chen, A.T. Alpas, Wear 1996; 192:186-98

[50] C.S. Ramesh, H. Adarsha, S. Pramod, Zulfiquar Khan, Materials and Design 50 (2013) 597-605

[51] B. Zahmatkesh, M.H. Enayati, Mater. Sci. Eng. A 527 (2010) 6734-6740

[52] B.L. Mordike, T. Ebert, Mater. Sci. Eng. A 302 (2001) 37-45

[53] M.-N. Avettand-Fènoël, A. Simar, R. Shabadi, R. Taillard, B. de Mesteer, Mater. Des. 60 (2014) 343-357

[54] A. Mertens, A. Simar, J. Adrien, E. Maire, H.-M. Montrieux, F. Delannay, J. Lecomte-Beckers, Materials Characterization 107 (2015) 125-133

[55] V.C. Gudla, F. Jensen, A. Simar, R. Shabadi, R. Ambat, Appl. Surf. Sci. 324 (2015) 554-562

[56] K. Nakata, S. Inoki, Y. Nagano, M. Ushio, Mater. Sci. Forum 426-432 (2003) 2873

[57] Omar S. Salih, Hengan Ou, W. Sun, D.G. McCartney, Materials and Design 86 (2015) 61-71

[58] Wenchao Yang, Shouxun Ji, Lanping Huang, Xiaofei Sheng, Zhou Li, Mingpu Wang, Materials Characterization 94 (2014) 170-177

[59] K. Razavizadeh, T.S. Eyre, Wear 79 (1982) 32

[60] K. Razavizadeh, T.S. Eyre, Wear 87 (1983) 261

[61] R. Antoniou, D.W. Borland, Mater. Sci. Eng. 93 (1987) 57

[62] K.N. Tandon, X.Y. Li, Scripta Mater. 38 (1998) 7

[63] J. Zhang, A.T. Alpas, Acta Mater. 45 (1997) 513

[64] A.R. Riahi, A.T. Alpas, Wear 251 (2001) 1396-1407

[65] F.F. Ling, E. Saibel, Wear 1, 801 957-958

[66] Y. Wei et al. Acta Metall. Sin. 47 (2011) 1535-1540

[67] M.L. Ted Guo, C.-Y.A. Tsao, Compos. Sci. Technol. 60 (1) (2000) 65-87

[68] Y. Wu el al., Wear 205 (1997) 64-70

[69] A. Dolata-Grosz, J. Wieczorek, Arch. Mater. Sci. Eng. 28 (3) (2007) 149-155

[70] A.P. Sannino, H.J. Rack, Wear 189 (1995) 1-19

[71] M. Kozma, in: 3rd national tribology conference, Galati, Romania (2003)

[72] A.T. Alpas, J. Zhang, Metall. Mater. Trans. A 25 (5) (1994) 969-983

[73] F. Gul, M. Acilar, Compos. Sci. Technol. 64(13-14) (2004) 1959-1970

[74] S.V. Prasad, R. Asthana, Tribol. Lett. 17 (3) (2004) 445

[75] K.R. Kumar et al., Sci. Eng. Compos. Mater. 19 (3) (2012) 247-253

[76] R. Purohit, G. Hemathkumar, R. Sgar, in: National seminar on emerging trends in manufacturing, Varanasi, India (2002)

[77] G. Hemath Kumar, in: International conference, Delhi, India (2003)

[78] S. Das et al., Aluminum Trans 2 (2000) 27-36

[79] S. Das, D.P. Mondal, G. Dixit, Metall. Mater. Trans. A 32 (3) (2001) 633-642

[80] S. Das et al., Wear 264 (2008) 47-59

[81] A.A. Cherit et al., Tribol. Ind. 30(3-4) (2008) 31-36

[82] K.V. Mahendra, K. Radhakrishna, J. Compos. Mater. 44 (8) (2010) 989-1005

[83] S. Basavajappa et al., J. Mater. Eng. Perform. 15 (6) (2006) 668-674

[84] S. Kumar, V. Balasubramanian, Tribol. Int. 43 (1-2) (2010) 414-422

[85] M. Baki Karamaş, F. Nair, Wear 265(11-12) (2008) 1741-1750

[86] M. Baki Karamaş et al. Wear 289 (2012) 73-81

[87] Q. Jun, A. Linan, P.J. Blau, in: STLE/ASME IJTC (2006)

[88] T. Wang, M. Shozaki, M. Yamamoto, A. Kagawa, Materials and Design (2015) 498-503

[89] Pradeep K. Rohatgi, Meysam Tabandeh-Khorshid, Emad Omrani, Micheal R. Lovell, Pradep L. Menez, Tribology for Scientists and Engineers: From Basics to Advanced Concepts, Chapter 8, P.L. Menezes et al. (eds.) (2013)

[90] F. Toptan, I. Kerti, L.A. Rocha, Wear 265 (2012) 74-85

[91] N. Natarajan, S. Vijayaranangan, I. Rajendran, Wear 261 (2006) 812-822

[92] G. Hemath Kumar et al., in: Frontiers in automobile and mechanical engineering, Chennai, India (2010)

[93] Y. Birol, Trans. Nonferrous Met. Soc. China 23 (2013) 1875-1881

[94] C.C. Degnan, P.H. Shipway, Mater. Sci. Technol. 18 (10) (2002) 1156-1162

[95] A. Vencl, A. Rac, I. Bobic, Tribol. Ind. 26 (3-4) (2004) 31-38

[96] D.P. Mondal, S. Das, Tribol. Ind. 39 (2008) 31-36

[97] K. Umanath, T.S. Selvamani, K Palanikumar, Int. J. Sci. Technol 3 (7) (2011) 5441-5451

[98] Y. Sahin, Mater. Des. 24 (2) (2003) 95-103

[99] M.J. Zhang et al., Trans. Nonferrous Metals Soc. China 20 (2010) 207-211

[100] N.Radhika, R. Subramanian, S. Venkat Prasat, J. Miner. Mater. Character. Eng. 10 (5) (2011) 427-443

[101] S. Zhang, F. Wang, J. Mater. Process. Technol. 182 (1-3) (2007) 122-127

[102] G. Ranganath, S.C. Sharma, Wear 251 (2001) 1408-1413

[103] S.K. Chaudhury et al., Wear 258 (2005) 759-769

[104] A.A. Hamid et al., Wear 265 (1-2) (2008) 14-26

[105] U. Soy, A. Demir, F. Findik, Industrial Lubrication and Technology 63 (5) (2011) 387-393

[106] H.J. Choi, S.M. Lee, D.H. Bae, Wear 270 (2010) 12-18

[107] A. Deschamps, Y. Bréchet, Acta Mater. 47 (1999) 293-305

[108] F.H. Stott, Tribology International 31 (1-3) (1998) 61-71

[109] J. Jiang, F.H. Stott, M.M. Stack, Wear 20 (1994) 185

[110] K.L. Johnson, K. Kendall, A.D. Roberts, Proc. R. Soc. London A324 (1971) 301

[111] I.N. Fridlyander, V.G. Sister, O.E Grushko, V.V. Berstenev, L.M. Sheveleva, L.A. Lvanova, Metal Sci. Heat Treat. 44 (2002) 356-370

[112] R. Nandan, T. DebRoy, H.K.D.H. Bhadeshia, Prog. Mater. Sci. 52 (2008) 980-1023

[113] O.S. Es-Said, J.G. Morris, H.D. Merchant, Metal. Mater. Trans. A 34 (2003) 751-763

[114] C. Gallais, Ph.D. Thesis, Institut National Polytechnique de Grenoble, France

[115] O. Lohne, A.L. Dons, Scand. J. Met. 12 (1983) 34-36

[116] W.F. Miao, D.E. Laughlin, Metal. Mater. Trans. A 31A (2000) 361

[117] A.K. Gupta, D.J. Loyd, S.A. Court, Mater. Sci. Eng. A 301 (2000) 140-146

[118] K. Matsuda, D. Teguri, Y. Uetani, T. Sato, S. Ikeno, Scripta Mater. 47 (2002) 833-837

[119] K. Matsuda, S. Ikeno, Y. Uetani, T. Sato, Metall. Mater. Trans. 32 (2006) 1293-1299

[120] D.J. Chakrabarti, D.E. Laughlin, Prog. Mater. Sci. 49 (2004) 389-410

[121] Wenchao Yang, Shoxun Ji, Lanping Huang, Xiaofei Sheng, Zhou Li, Mingpu Wang, Mater. Char. 94 (2014) 170-177

[122] Wenyi Yan, Noel P. O'Dowd, Esteban P. Busso, J. Mech. Phys. Solids 50 (2002) 449-470

[123] ASM Handbook Vol. 9 Metallography and Microstructures, Materials Park (OH), 9th edition (1998)